2023

Lipid binding properties of huntingtin as a novel therapeutic target

Chathuranga Siriwardhana
West Virginia University, ccs0019@mix.wvu.edu

Lipid binding properties of huntingtin as a novel therapeutic target

Chathuranga Siriwardhana

Dissertation submitted to the
Eberly college of Arts and Science
at West Virginia University
in partial fulfilment of the requirements for the degree of

Doctor in Philosophy
in
Chemistry

Justin Legleiter, Ph.D., Committee chairperson

Blake Mertz, Ph.D.

Werner Geldenhuys, Ph.D.

Brian Popp, Ph.D.

Kenneth Showalter, Ph.D.

C. Eugene Bennett Department of Chemistry

Morgantown, West Virginia

2023

Keywords: huntingtin, lipid membranes, membrane damage, amyloid neurodegenerative diseases, protein lipid interaction

Abstract

Lipid binding properties of huntingtin as a novel therapeutic target

Chathuranga Siriwardhana

As protein aggregation is the defining hallmark of all amyloid diseases, a common therapeutic strategy is to develop molecules that inhibit aggregation. However, this approach has yielded limited success. Many amyloid proteins directly interact with lipid membranes. These interactions promote distinct aggregation pathways and often result in membrane damage leading to toxicity. As a result, directly targeting the ability of amyloids to bind lipid membranes represents a novel therapeutic strategy. As a proof of principle, the interaction between lipid membranes and mutant huntingtin protein (htt) aggregates was used to test this strategy. Mutant htt containing an expanded polygulatmine (polyQ) domain causes Huntington's disease (HD). Using a colorimetric lipid binding assay over 1200 compounds were screened for their ability to block htt/lipid binding. The screen was set up to only identify compounds that directly interacted with htt, not the lipid membrane. Three compounds were identified having the ability to inhibit htt/lipid interaction, Ro-90-7501 (Ro), benzamil hydrochloride (ben) and ruthenium red. As these compounds directly interact with htt, ThT and AFM assays were performed to assess their impact on aggregation. Ro and ben did not inhibit fibril formation; however, oligomer precursors were significantly smaller when exposed to Benzamil. Molecular dynamic simulations (MD) revealed that the two compounds have unique mechanisms of interaction with htt aggregates. Unlike Ro and ben, ruthenium red altered htt aggregation and inhibit fibrilization. Having established that the compound prevented htt from binding membranes, a *C. elegans* model of HD was used to determine if this strategy could

alleviate phenotype. Despite have a minimal impact on punctate formation, all three compounds reduced a thrashing deficit in animals caused by mutant htt expression, suggesting that this strategy reduces htt toxicity.

Acknowledgement

I would like to express my heartfelt gratitude to Dr. Justin Legleiter, my advisor, for his guidance, encouragement, and unwavering support throughout my PhD journey. Your expertise and insights have been invaluable in shaping my research and refining my ideas. Your mentorship has been invaluable. I'm grateful for your ultimate patience and understanding with me during our discussions. Thank you for everything you did to make me in to a better researcher.

I am also deeply grateful to Dr. Geldenhyus and Dr. Mertz for their valuable advice and feedback, which helped me to develop my research in new and innovative ways. I extend by appreciation to other committee members Dr. Popp and Dr. Showalter for their dedication of time and advice.

Special thanks go to my lab members Dr. Adegbuyiro, Dr. Sedighi, Dr. Groover, Dr. Beasley, Dr. Stonebraker, Adam Skeens for your collaborations, insights, and support. I'm also thankful to Chidi, Anjola and Gabriella.

A special thanks goes to my wife, Hansika Herath, for her unwavering love, support, and patience throughout this journey. Her encouragement and belief in me have been a constant source of strength and inspiration.

Finally, I would like to express my gratitude to my friends and family for their unwavering support, encouragement, and belief in me. Their love, guidance, and support have been instrumental in shaping who I am today, and I am forever grateful for their presence in my life.

Table of Content

List of Figures

List of abbreviations

AD	Alzheimer's disease
AFM	Atomic force microscopy
Aβ	Amyloid beta
ben	Benzamil hydrochloride
C.elegans	*Caenorhabditis elegans*
CR	Colorimetric response
DMPC	1,2-Dimyristoyl-sn-glycero-3-phosphocholine
DOPC	1,2-Dioleoyl-sn-glycero-3-phosphocholine
ER	Endoplasmic reticulum
GST	Glutathione-S-trasferase
HD	Huntington's disease
htt	huntingtin
htt-exon1(46Q)	huntingtin exon1 with 46 glutamines
Kda	Kilo Dalton
MD	Molecular dynamics
Nt17	First 17 amino acids of huntingtin exon1
PD	Parkinson's disease
PDA	Poly diacetylene
PolyP	Poly proline
PolyQ	Poly glutamine
POPC	1-palmitoyl-2-oleoyl-sn-glycero-3-phosphocholine
POPE	1-Palmitoyl-2-oleoyl-sn-glycero-3-phosphatidylethanolamine
POPG	1-Palmitoyl-2-oleoyl-sn-glycero-3-phosphatidylglycerol
POPS	1-palmitoyl-2-oleoyl-sn-glycero-3-phospho-L-serine
PPII	Polyproline helix
Ro	Ro-90-7501
SDS	Sodium dodecyl sulfate
SEM	Standard error mean
TBLE	Total brain lipid extract
TBS	Tris buffered saline
ThT	Thioflavin T
YFP	Yellow fluorescent protein
α-syn	Apha syneuclien

Chapter 1 Protein aggregation and lipid interaction in Huntington's disease

1.1 Overview

Many neurodegenerative diseases are associated with the rearrangement of a specific proteins into non-native conformations which result in the formation of abnormal fibrous, extracellular, proteinaceous deposits found in cellular compartments and tissues[1]. These are referred to as amyloids. Amyloid aggregation is a complex phenomenon that yields a mixture of heterogeneous aggregate species ranging from small oligomers to larger fibrils[2–4]. The process is influenced by the presence of cellular and subcellular membranes, which are predominantly comprised of lipids. Many amyloid forming proteins and their aggregates directly bind and disrupt membranes resulting in dysfunction of neuronal activities, eventually causing cell death[5–7]. This suggest that blocking the interaction between amyloid protein (and aggregates) and membranes is feasible therapeutic strategy.

1.2 Amyloid disorders

A commonality in vast majority of the neurodegenerative diseases such as Alzheimer's diseases (AD), Parkinson's diseases (PD) and Huntington's (HD) is the deposition of a specific proteinaceous aggregates in cellular compartments and tissues[8,9]. These proteins are` organized into fibrillar aggregates with a cross β-structure which are referred to as amyloids. Amyloid aggregates are highly stable, SDS insoluble, and resistant to proteolytic degradation[10–12]. Apart from the formation of fibrillar aggregates a variety of intermediate aggregates form which includes small oligomers, protofibrils, amorphous aggregates, and annular aggregates[13–16]. Many of these aggregate species are associated with toxic gain of function. For example, injection of fibrilized β-amyloid

(Aβ) in rat hippocampus impairs synaptic transmission and memory deficit[17]. Moreover, soluble Aβ oligomers bind to synapses damaging neurons[18]. Both huntingtin and α-synuclein fibrils cause toxicity in cultured cells leading to apoptotic cell death[19].

Amyloid aggregation is a free energy driven process similar to normal protein folding in cellular environment. A newly expressed protein progress along an energy landscape, folding into a minimal energy conformation which is known as the native state, based on the amino acid sequence[20,21] (Figure1). During protein folding the minimal energy is obtained by sequestering hydrophobic residues inside a hydrophilic core of the protein structure[22,23]. However, due to misfolding, proteins can become trapped in local energy minima. This causes the formation of smaller aggregates oligomers. Eventually, oligomers can structurally reorganize into the more stable β-sheet rich oligomers and amyloid fibrils[24]. Amyloid fibrils are enthalpically stable due to the formation of a network of hydrogen bonds formed between β-sheets that holds them together[25]. These aggregates accumulate in neurons causing the advent of amyloid-based neurodegenerative diseases.

As amyloid aggregation is the major hallmark of these diseases, a variety of strategies have been pursued to modify or slow the aggregation process. One such approach is the development of antibodies that are capable of binding to amyloid-forming proteins and resulting aggregates. Bapineuzumab, Crenezumab, Gantenerumab and Solanezumab are antibodies specific for multiple aggregate forms of Aβ which is the protein responsible for AD[26–28]. However, none of these antibodies displayed great effectiveness in treating AD in clinical trials. [29] Another approach is the development of small molecules. EGCG, curcumin, Congo red, and riluzole are some examples of such

molecules which are developed to alter amyloid aggregation of Aβ, α-synuclein (PD) and huntingtin (HD) proteins[30–33] . While these molecules clearly reduce fibril formation *in vitro,* many of them are therapeutic dead ends for a variety of reasons. For example, EGCG has limited bioavailability[34].

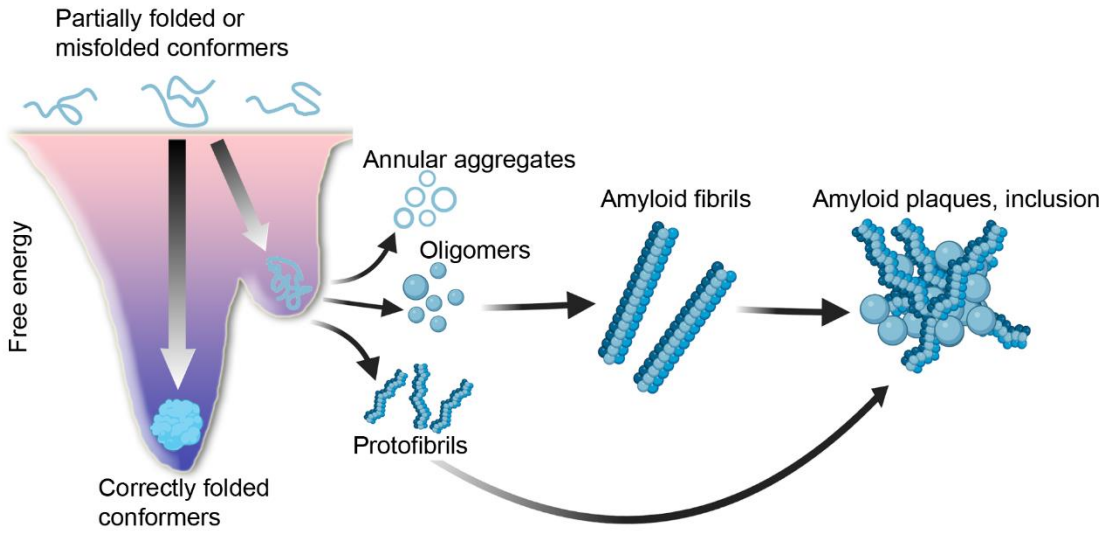

Figure 1.1 Aggregation scheme for amyloid forming proteins, Proteins typically folds into the native configuration which is minimal in free energy. However, due to a variety of possibilities, proteins can get misfolded and trapped in local energy minima leading to a heterogeneous mixture of aggregates such as oligomers, protofibrils etc. These aggregates eventually develop in to β-sheet rich amyloid fibrils. Aggregated proteins accumulate into amyloid plaques or inclusion in neurons in the brain.

Aggregation of many amyloid proteins is altered in the presence of lipid membranes. For example, fibrilization of α-syneuclein and islet amyloid polypeptide fibrilization is enhanced in the presence of lipid membranes[35,36]. Depending on lipid composition, huntingtin aggregation is suppressed or enhanced in the presence of membranes[37]. Multiple lines of evidence support the notion that amyloid-forming proteins and their aggregates bind to and damage membranes. Aβ disrupts lipid membranes bot *in vivo* and *in vitro*[5,38]*.* α-syneuclein interacts with multiple organelle membranes,

especially mitochondria, resulting in cellular toxicity[7,39]. Moreover, htt inclusions impinge nuclear envelope resulting in cell death[40].

1.3 Huntington's disease and huntingtin (htt) aggregation

While several factors can induce proteins to form amyloid, there are a subset of genetic amyloid-based neurodegenerative diseases caused by an expansion of a polylutamine (polyQ) domain within specific proteins. Of these diseases, HD is the most common. HD is an autosomal dominant genetic disorder caused by a mutation in the IT15 gene present in short arm of chromosome 4[41,42]. This gene encodes for huntingtin protein (htt) and the mutation is caused due to an expansion of a trinucleotide repeat unit CAG that encodes for the poly polyQ stretch near N-terminus of htt. The normal polyQ tract of htt is ~17-20 glutamine repeats units, while the threshold for the disease is above 35 repeats[43,44]. PolyQ length has a strong correlation with the age of onset and the severity of the disease. The longer the repeat length, the earlier the onset of the disease. Typical onset (21-50 years old) of the disease occurs with a median polyQ length of 45, late onset (above 50 years old) occurs with a median polyQ length of 42, while early onset (2-20 years old) occurs with a median polyQ length of 60[45]. Phenotype manifest in patients as chorea, depression, cognitive loss, and behavioral abnormalities[46–49].

Htt is a multifunctional protein ~350 kDa in size and having ~3144 amino acids[50]. Htt plays a role in vesicles and organelle transport[51,52]. Wildtype htt also demonstrate antiapoptotic activity during proapoptotic challenges[53,54].Further htt is associated with transcriptional regulation[55,56]. With regard to HD, the first exon of htt (htt-exon1) and other N-terminal fragments containing polyQ are linked with toxicity. For example, HD phenotype was observed in transgenic mouse models that expresses htt-exon1. This

resulted in morphological changes in neuronal nuclei which is similar to neuronal abnormalities in HD patients neurons [57]. Expression of N-terminus exon 1 resulted in mitochondrial dysfunction and disruption of ER functions[58,59]. Additionally, aggregates of N-terminus fractions were identified in human postmortem brains of HD[60]. In htt-exon1 the polyQ stretch is flanked by a domain consisting of 17 amino acids (Nt17) and a proline rich domain consisting of two poly proline (polyP) stretches towards its C-terminus[61]. Both of these flanking sequences influence htt aggregation which will be discussed in depth in section 1.5

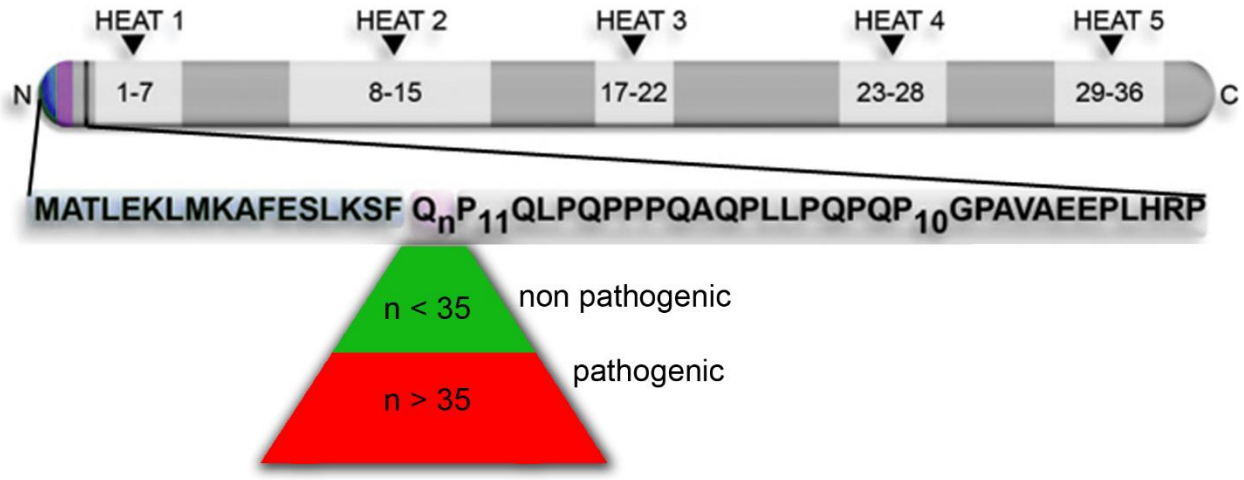

Figure 1.2 Full length htt protein containing several HEATS and flanking sequence of polyQ and pathogenic polyQ length, PolyQ is flanked on its N-terminus by 17 amino acids (shaded in blue) which is identified as Nt17 and a proline rich domain on its C-terminus (shaded in grey). Below 35 glutamines in the polyQ stretch is non pathogenic and exceeding the threshold of 35 glutamines is pathogenic causing the disease.

Htt aggregation follows a multi-step pathway similar to other amyloids. The aggregation starts with a lag phase where a critical nucleus forms from monomeric or multimeric htt[1,62]. Time of the lag phase depends on a variety of factors especially the

polyQ length. It is observed that a shorter polyQ stretch results in a longer lag phase, while a longer polyQ stretch results in a shorter lag phase[63]. This step is followed by an elongations phase which causes in extensive growth of fibrils. A plateau phase results after the elongation phase which represents a steady state when a majority of monomers are transformed to β-sheet rich fibrils[62]. The process of polyQ aggregation is complex, involving multiple pathways that are not mutually exclusive. The pathways that result in the formation of fibrils are referred to as “on pathways”. The two major on pathways are 1. Direct nucleation of monomers to fibrils[63,64] and 2. Formation of oligomeric intermediates that leads to β-sheet rich fibrillar structures[14,16,65]. There are also several other “off pathways” that can lead to the formation of oligomers of different sizes, annular aggregates and amorphous aggregates. All these higher aggregates eventually coalesce into inclusion, which is a hallmark of HD. Because of the complexity of aggregation, a heterogeneous mixture of aggregates co-exists in the cellular environment[14].

1.4 Toxicity associated with htt aggregation

The formation of inclusion bodies may represent a protective cellular response by sequestering diffuse htt aggregates. Inclusion formation in striatal neurons does not corelate with huntingtin induced cell death, and suppressing inclusion formation in cells expressing mutant htt increases cell death[66]. Survival analysis of neurons performed using robotic microscopes that can track the fate of individual neurons over long time periods provides further evidence of a protective role for inclusion formation[67]. In short, neurons that formed htt inclusions early had a significantly reduced risk of death compared to neurons in which htt remained diffusely distributed. As state earlier, the diffuse fraction of htt within cells consists of a variety of aggregate species that co-exist.

As a result, unraveling the potential role for different aggregate specie in cellular toxicity is difficult.

The toxicity associated with each aggregate type continues to be debated. The heterogeneous nature of htt aggregation makes it difficult to determine which aggregate species are the most toxic. Smaller diffused aggregate species ranging from oligomers to small fibrils are identified to be associated with significant toxicity[68]. Many studies suggest that soluble oligomers, not mature fibrils, are the main toxic agents in HD[69,70]. Using microscopic techniques and immunochemical assays, it was confirmed that oligomers are formed in the brains of mutant R6/2 and HdhQ150 knock -in mice which are morphologically similar to the htt oligomers formed *in vitro*[71]. However, htt oligomers tend to disappear overtime with the formation of inclusion bodies[72]. Furthermore, oligomer disrupt brain lipid bilayers[73] and cause ER stress[74]. However, fibrils are also associated with HD toxicity. For instance, fibrils trigger apoptosis by binding and disrupting lipid membranes[19]. Moreover, the formation of β-sheet rich fibrils strongly correlates with toxic in neuronal cells and Drosophila flies that express mutant htt[75]. In light of these facts, it is difficult to determine the relative roles and mechanism of specific aggregate species in HD.

1.5 Flanking sequence influence htt aggregation

The flanking sequence adjacent to the polyQ domain alter htt aggregation[16,76–79]. The polyP domain slows aggregation *in vitro.* Addition of a 10 residue proline domain at the C-terminus of polyQ significantly decreases htt aggregation[16,80–82]. However, addition of polyP at the N-terminus does not modulate polyQ aggregation[80]. The polyP domain typically has a PPII like helical structure and this helicity is propagated to the polyQ

domain from the C-terminal side[82]. However, this helicity propagation into the polyQ domain is not observed in fibrls, suggesting it is lost during the course of aggregation[83].

Htt aggregation is also influenced by Nt17, which accelerates fibril formation peptides[16]. The mechanism by which Nt17 enhances fibril formation is based on intermolecular self-association between monomers by the formation of an amphipathic α-helix[84–88]. Nt17 at low concentrations is intrinsically disordered in ionic buffer solution but can undergo a conformational transformation into an amphipathic α-helix (AH) in the presence of a binding partner[77,89]. Hydrophobic phases interact when multiple Nt17 AHs are closer in proximity, forming helical bundles leading to the formation of α-helical oligomers[77]. This shifts the aggregation mechanism toward an oligomer-mediated pathway[16,90,91]. Nt17 mediated oligomer formation brings the polyQ tracts into close proximity, lowering the barrier to nucleation[16,77,92]. In support of this mechanism, Nt17 peptides (without polyQ attached) inhibits aggregation of htt when co-incubated with htt peptides[87]. That is, incorporation of these free Nt17 peptides into oligomers increases the intermolecular spacing between polyQ tracts, creating a larger energy barrier to nucleation. Unlike polyp, the impact of Nt17 on htt aggregation is independent of position, as Nt17 lociated on either the N-terminal or C-terminal side of polyQ can trigger aggregation[93]. It is also important to note that Nt17 maintains α-helicity in the fibril structure[94].

1.6 Htt-lipid interaction

Expansion of polyQ enhances the localization of htt to cellular membranes and increase the extent of htt-associated membrane damage. Oligomers of N-terminal htt fragments reside in postsynaptic membranes of R6/2 transgenic mouse brains[73]. In cell

lines expressing expanded polyQ, perinuclear inclusions of htt impinge and distort nuclear membranes resulting in neuronal death[40]. Furthermore, htt distorts, degrades, and damages ER membranes resulting in Bax insertion causing cell death[95]. Htt also directly binds to acidic phospholipid membranes of plasma membrane[96]. In a recently developed pig model of HD, both mitochondrial membranes and nuclear envelopes are distorted[97]. Furthermore, mutant htt alters mitochondrial membrane potential and mitochondrial fission[98]. Htt inclusions contain fractions of the various membranous structures such as ER and mitochondria[99,100]. Independent of the polyQ length localization of htt is observed in variety of subcellular compartments like endosomes, synaptic vesicles and dendritic plasma membrane[101].

The Nt17 amphipathic α-helix serves as the lipid binding domain of htt-exon1[88,102]. Synthetic polyQ peptides lacking Nt17 do not interact with lipid vesicles or model membranes, suggesting Nt17 is crucial for htt lipid binding[103]. Computational studies have revealed a stepwise mechanism of Nt17 lipid membrane interaction[104,105]. The first step is driven by long range electrostatic interactions between Nt17 and lipid head groups. This interaction is mainly driven via charged amino acids residues such as lysine. It is followed by a reorganizing step resulting in a structural change that brings nonpolar residues near the membrane core. During this step uncoiling of the α-helix can occur. Then an anchoring step occurs where nonpolar residues such as phenylalanine move towards the core of the lipid membrane. Finally other non-polar residues are partitioned into the membrane. Furthermore, Nt17 membrane association modulates htt aggregation[86,106]. This is due to the increase of high local concentration of polyQ near the

membrane surface when multiple htt monomers are bound to membrane. However, this depends on lipid composition[37].

1.7 Dissertation outline and rationale

Amyloid related neurodegenerative diseases affect millions of people worldwide. In 2019 WHO estimated that globally, there were over 50 million people living with AD or other dementia[107]. One in three seniors dies with AD or related dementia[108]. Nearly one million people in the U.S. are living with PD. This number is expected to rise to 1.2 million by 2030. Experts estimate that one in every 10,000 persons-nearly 30,000 in the United States-have HD and these numbers are increasing. These statistics indicate a critical need for the discovery of novel therapeutics for these diseases.

Since aggregation of proteins into fibrils that deposits in cells is a major hallmark of many neurodegenerative diseases, scientists have been conducting extensive research on identifying and developing methods to suppress aggregate formation. Despite this, none of these strategies have led to the discovery of successful therapeutics. Instead, a recent failure in phase 3 clinical trial of monoclonal antibodies for AD was reported[109]. Consequently, focusing on other aspects of amyloids instead of aggregation is urgently needed. As many amyloids bind and damage membranes, an innovative therapeutic strategy may be blocking amyloid/lipid interactions. Here, using mutant htt as a model system, the feasibility of this strategy is evaluated and proof of principle is provided. Over 1200 compounds were screened for their ability to block htt lipid interaction. 15 compounds were initially identified and 6 were validated with secondary assays. Of the six identified compounds, three compounds were selected for further analysis.In chapter 2, identification of the candidate compounds via a lipid binding screen

is described along with the investigation of two compounds: Ro 90-7501 (Ro) and Benzamil hydrochloride (Ben). This chapter provides mechanistic insight into the interaction of these compounds with htt and demonstrates that this strategy can improve phenotype in a *C. elegans* model of HD. Importantly, this improvement occurred despite neither compound inhibiting fibril formation. As opposed to Ro and Ben, ruthenium red inhibited the formation of Htt fibrils while inhibiting the interaction between htt and lipids. As a result, the interaction of ruthenium red with htt is explored in chapter 3. Collectively, these studies provide a clear roadmap for applying this approach in drug discovery for other amyloid-based diseases.

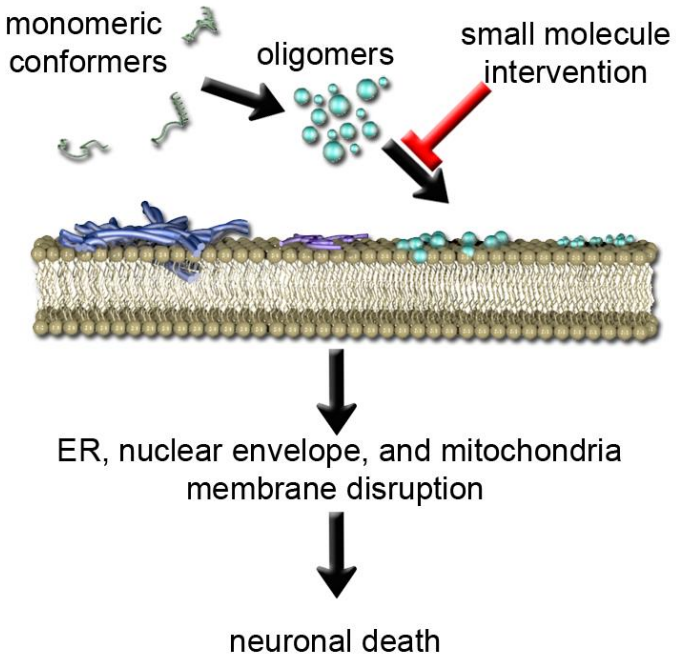

Figure 1.3 Targeting the ability of htt to bind lipid membranes as a novel therapeutic strategy.

1.8 References

1. Chiti, F. & Dobson, C. M. Protein Misfolding, Functional Amyloid, and Human Disease. *Annu. Rev. Biochem.* **75**, 333–366 (2006).
2. Banerjee, S. *et al.* Nanoscale Infrared Spectroscopy Identifies Structural Heterogeneity in Individual Amyloid Fibrils and Prefibrillar Aggregates. *J. Phys. Chem. B* **126**, 5832–5841 (2022).
3. Sahoo, B. R., Cox, S. J. & Ramamoorthy, A. High-resolution probing of early events in amyloid-β aggregation related to Alzheimer's disease. *Chem. Commun.* **56**, 4627–4639 (2020).
4. Lotz, G. P. & Legleiter, J. The role of amyloidogenic protein oligomerization in neurodegenerative disease. *J Mol Med* **91**, 653–664 (2013).
5. Burke, K. A., Yates, E. A. & Legleiter, J. Biophysical Insights into How Surfaces, Including Lipid Membranes, Modulate Protein Aggregation Related to Neurodegeneration. *Front. Neurol.* **4**, (2013).
6. Yasumoto, T. *et al.* High molecular weight amyloid $\beta_{1\text{-}42}$ oligomers induce neurotoxicity *via* plasma membrane damage. *FASEB j.* **33**, 9220–9234 (2019).
7. Ericsson, M. *et al.* Crowded organelles, lipid accumulation, and abnormal membrane tubulation in cellular models of enhanced α-synuclein membrane interaction. *Brain Research* **1758**, 147349 (2021).
8. Chen, L. & Feany, M. B. α-Synuclein phosphorylation controls neurotoxicity and inclusion formation in a Drosophila model of Parkinson disease. *Nat Neurosci* **8**, 657–663 (2005).
9. Roos, R. A. Huntington's disease: a clinical review. *Orphanet J Rare Dis* **5**, 40 (2010).
10. Dobson, C. M. Protein misfolding, evolution and disease. *Trends in Biochemical Sciences* **24**, 329–332 (1999).
11. Carrell, R. W. & Lomas, D. A. Conformational disease. *The Lancet* **350**, 134–138 (1997).
12. Soto, C. Unfolding the role of protein misfolding in neurodegenerative diseases. *Nat Rev Neurosci* **4**, 49–60 (2003).
13. Poirier, M. A. *et al.* Huntingtin Spheroids and Protofibrils as Precursors in Polyglutamine Fibrilization. *Journal of Biological Chemistry* **277**, 41032–41037 (2002).
14. Legleiter, J. *et al.* Mutant Huntingtin Fragments Form Oligomers in a Polyglutamine Length-dependent Manner in Vitro and in Vivo. *Journal of Biological Chemistry* **285**, 14777–14790 (2010).
15. Jayaraman, M. *et al.* Kinetically Competing Huntingtin Aggregation Pathways Control Amyloid Polymorphism and Properties. *Biochemistry* **51**, 2706–2716 (2012).
16. Thakur, A. K. *et al.* Polyglutamine disruption of the huntingtin exon 1 N terminus triggers a complex aggregation mechanism. *Nat Struct Mol Biol* **16**, 380–389 (2009).
17. Stéphan, A., Laroche, S. & Davis, S. Generation of Aggregated β-Amyloid in the Rat Hippocampus Impairs Synaptic Transmission and Plasticity and Causes Memory Deficits. *J. Neurosci.* **21**, 5703–5714 (2001).
18. Lacor, P. N. *et al.* Aβ Oligomer-Induced Aberrations in Synapse Composition, Shape, and Density Provide a Molecular Basis for Loss of Connectivity in Alzheimer's Disease. *J. Neurosci.* **27**, 796–807 (2007).

19. Pieri, L., Madiona, K., Bousset, L. & Melki, R. Fibrillar α-Synuclein and Huntingtin Exon 1 Assemblies Are Toxic to the Cells. *Biophysical Journal* **102**, 2894–2905 (2012).
20. Wolynes, P. G., Onuchic, J. N. & Thirumalai, D. Navigating the Folding Routes. *Science* **267**, 1619–1620 (1995).
21. Dill, K. A. & Chan, H. S. From Levinthal to pathways to funnels. *Nat Struct Mol Biol* **4**, 10–19 (1997).
22. Dinner, A. R., Šali, A., Smith, L. J., Dobson, C. M. & Karplus, M. Understanding protein folding via free-energy surfaces from theory and experiment. *Trends in Biochemical Sciences* **25**, 331–339 (2000).
23. Anfinsen, C. B. The formation and stabilization of protein structure. *Biochemical Journal* **128**, 737–749 (1972).
24. Vendruscolo, M., Paci, E., Karplus, M. & Dobson, C. M. Structures and relative free energies of partially folded states of proteins. *Proc. Natl. Acad. Sci. U.S.A.* **100**, 14817–14821 (2003).
25. Wetzel, R. Kinetics and Thermodynamics of Amyloid Fibril Assembly. *Acc. Chem. Res.* **39**, 671–679 (2006).
26. Faber, P. W., Alter, J. R., MacDonald, M. E. & Hart, A. C. Polyglutamine-mediated dysfunction and apoptotic death of a Caenorhabditis elegans sensory neuron. *Proceedings of the National Academy of Sciences* **96**, 179–184 (1999).
27. Kerchner, G. A. & Boxer, A. L. Bapineuzumab. *Expert Opinion on Biological Therapy* **10**, 1121–1130 (2010).
28. Ultsch, M. *et al.* Structure of Crenezumab Complex with Aβ Shows Loss of β-Hairpin. *Sci Rep* **6**, 39374 (2016).
29. Tian Hui Kwan, A., Arfaie, S., Therriault, J., Rosa-Neto, P. & Gauthier, S. Lessons Learnt from the Second Generation of Anti-Amyloid Monoclonal Antibodies Clinical Trials. *Dement Geriatr Cogn Disord* **49**, 334–348 (2020).
30. Palhano, F. L., Lee, J., Grimster, N. P. & Kelly, J. W. Toward the Molecular Mechanism(s) by Which EGCG Treatment Remodels Mature Amyloid Fibrils. *J. Am. Chem. Soc.* **135**, 7503–7510 (2013).
31. Ehrnhoefer, D. E. *et al.* EGCG redirects amyloidogenic polypeptides into unstructured, off-pathway oligomers. *Nat Struct Mol Biol* **15**, 558–566 (2008).
32. Pandey, N., Strider, J., Nolan, W. C., Yan, S. X. & Galvin, J. E. Curcumin inhibits aggregation of α-synuclein. *Acta Neuropathol* **115**, 479–489 (2008).
33. Ren, S.-C. *et al.* Riluzole prevents soluble A **β** $_{1–42}$ oligomers-induced perturbation of spontaneous discharge in the hippocampal CA1 region of rats. *Amyloid* **22**, 36–44 (2015).
34. Andreu Fernández, V. *et al.* Bioavailability of Epigallocatechin Gallate Administered with Different Nutritional Strategies in Healthy Volunteers. *Antioxidants* **9**, 440 (2020).
35. Knight, J. D. & Miranker, A. D. Phospholipid Catalysis of Diabetic Amyloid Assembly. *Journal of Molecular Biology* **341**, 1175–1187 (2004).
36. Jo, E. *et al.* α-Synuclein-synaptosomal membrane interactions: Implications for fibrillogenesis. *European Journal of Biochemistry* **271**, 3180–3189 (2004).
37. Beasley, M. *et al.* Physicochemical Properties Altered by the Tail Group of Lipid Membranes Influence Huntingtin Aggregation and Lipid Binding. *J. Phys. Chem. B* **126**, 3067–3081 (2022).

38. Yip, C. M. & McLaurin, J. Amyloid-β Peptide Assembly: A Critical Step in Fibrillogenesis and Membrane Disruption. *Biophysical Journal* **80**, 1359–1371 (2001).
39. Fusco, G. *et al.* Structural basis of membrane disruption and cellular toxicity by α-synuclein oligomers. *Science* **358**, 1440–1443 (2017).
40. Liu, K.-Y. *et al.* Disruption of the nuclear membrane by perinuclear inclusions of mutant huntingtin causes cell-cycle re-entry and striatal cell death in mouse and cell models of Huntington's disease. *Human Molecular Genetics* **24**, 1602–1616 (2015).
41. Nørremølle, A. *et al.* Trinucleotide repeat elongation in the Huntingtin gene in Huntington Disease patients from 71 Danish families. *Hum Mol Genet* **2**, 1475–1476 (1993).
42. Macdonald, M. A novel gene containing a trinucleotide repeat that is expanded and unstable on Huntington's disease chromosomes. *Cell* **72**, 971–983 (1993).
43. Penney, J. B., Vonsattel, J.-P., Macdonald, M. E., Gusella, J. F. & Myers, R. H. CAG repeat number governs the development rate of pathology in Huntington's disease. *Ann Neurol.* **41**, 689–692 (1997).
44. Snell, R. G. *et al.* Relationship between trinucleotide repeat expansion and phenotypic variation in Huntington's disease. *Nat Genet* **4**, 393–397 (1993).
45. The U.S.-Venezuela Collaborative *et al.* Venezuelan kindreds reveal that genetic and environmental factors modulate Huntington's disease age of onset. *Proceedings of the National Academy of Sciences* **101**, 3498–3503 (2004).
46. Anderson, K. E. & Marder, K. S. An overview of psychiatric symptoms in Huntington's disease. *Curr Psychiatry Rep* **3**, 379–388 (2001).
47. Papoutsi, M., Labuschagne, I., Tabrizi, S. J. & Stout, J. C. The cognitive burden in Huntington's disease: Pathology, phenotype, and mechanisms of compensation: The Cognitive Burden in Hd. *Mov Disord.* **29**, 673–683 (2014).
48. Myrianthopoulos, N. C. Huntington's Chorea. *Journal of Medical Genetics* **3**, 298–314 (1966).
49. Paulsen, J. S., Miller, A. C., Hayes, T. & Shaw, E. Cognitive and behavioral changes in Huntington disease before diagnosis. in *Handbook of Clinical Neurology* vol. 144 69–91 (Elsevier, 2017).
50. Cornett, J. *et al.* Polyglutamine expansion of huntingtin impairs its nuclear export. *Nat Genet* **37**, 198–204 (2005).
51. Caviston, J. P. & Holzbaur, E. L. F. Huntingtin as an essential integrator of intracellular vesicular trafficking. *Trends in Cell Biology* **19**, 147–155 (2009).
52. Trushina, E. *et al.* Mutant Huntingtin Impairs Axonal Trafficking in Mammalian Neurons In Vivo and In Vitro. *Mol Cell Biol* **24**, 8195–8209 (2004).
53. Leavitt, B. R. *et al.* Wild-Type Huntingtin Reduces the Cellular Toxicity of Mutant Huntingtin In Vivo. *The American Journal of Human Genetics* **68**, 313–324 (2001).
54. Rigamonti, D. *et al.* Wild-Type Huntingtin Protects from Apoptosis Upstream of Caspase-3. *J. Neurosci.* **20**, 3705–3713 (2000).
55. Cha, J.-H. J. Transcriptional signatures in Huntington's disease. *Progress in Neurobiology* **83**, 228–248 (2007).
56. Zucker, B. *et al.* Transcriptional dysregulation in striatal projection- and interneurons in a mouse model of Huntington's disease: neuronal selectivity and potential neuroprotective role of HAP1. *Human Molecular Genetics* **14**, 179–189 (2005).

57. Davies, S. W. *et al.* Formation of Neuronal Intranuclear Inclusions Underlies the Neurological Dysfunction in Mice Transgenic for the HD Mutation. *Cell* **90**, 537–548 (1997).
58. De Mario, A. *et al.* Calcium Handling by Endoplasmic Reticulum and Mitochondria in a Cell Model of Huntington's Disease. *PLoS Curr* (2016) doi:10.1371/currents.hd.37fcb1c9a27503dc845594ee4a7316c3.
59. Ghosh, R. *et al.* Expression of mutant exon 1 huntingtin fragments in human neural stem cells and neurons causes inclusion formation and mitochondrial dysfunction. *FASEB j.* **34**, 8139–8154 (2020).
60. DiFiglia, M. *et al.* Aggregation of Huntingtin in Neuronal Intranuclear Inclusions and Dystrophic Neurites in Brain. *Science* **277**, 1990–1993 (1997).
61. Adegbuyiro, A., Sedighi, F., Pilkington, A. W., Groover, S. & Legleiter, J. Proteins Containing Expanded Polyglutamine Tracts and Neurodegenerative Disease. *Biochemistry* **56**, 1199–1217 (2017).
62. Xue, W.-F., Homans, S. W. & Radford, S. E. Systematic analysis of nucleation-dependent polymerization reveals new insights into the mechanism of amyloid self-assembly. *Proc. Natl. Acad. Sci. U.S.A.* **105**, 8926–8931 (2008).
63. Chen, S., Berthelier, V., Yang, W. & Wetzel, R. Polyglutamine aggregation behavior in vitro supports a recruitment mechanism of cytotoxicity. *Journal of Molecular Biology* **311**, 173–182 (2001).
64. Chen, S., Berthelier, V., Hamilton, J. B., O'Nuallai, B. & Wetzel, R. Amyloid-like Features of Polyglutamine Aggregates and Their Assembly Kinetics. *Biochemistry* **41**, 7391–7399 (2002).
65. Walters, R. H. & Murphy, R. M. Examining Polyglutamine Peptide Length: A Connection between Collapsed Conformations and Increased Aggregation. *Journal of Molecular Biology* **393**, 978–992 (2009).
66. Saudou, F., Finkbeiner, S., Devys, D. & Greenberg, M. E. Huntingtin Acts in the Nucleus to Induce Apoptosis but Death Does Not Correlate with the Formation of Intranuclear Inclusions. *Cell* **95**, 55–66 (1998).
67. Arrasate, M., Mitra, S., Schweitzer, E. S., Segal, M. R. & Finkbeiner, S. Inclusion body formation reduces levels of mutant huntingtin and the risk of neuronal death. *Nature* **431**, 805–810 (2004).
68. Xi, W., Wang, X., Laue, T. M. & Denis, C. L. Multiple discrete soluble aggregates influence polyglutamine toxicity in a Huntington's disease model system. *Sci Rep* **6**, 34916 (2016).
69. Lajoie, P. & Snapp, E. L. Formation and Toxicity of Soluble Polyglutamine Oligomers in Living Cells. *PLoS ONE* **5**, e15245 (2010).
70. Kim, Y. E. *et al.* Soluble Oligomers of PolyQ-Expanded Huntingtin Target a Multiplicity of Key Cellular Factors. *Molecular Cell* **63**, 951–964 (2016).
71. Sathasivam, K. *et al.* Identical oligomeric and fibrillar structures captured from the brains of R6/2 and knock-in mouse models of Huntington's disease. *Human Molecular Genetics* **19**, 65–78 (2010).
72. Marcellin, D. *et al.* Fragments of HdhQ150 Mutant Huntingtin Form a Soluble Oligomer Pool That Declines with Aggregate Deposition upon Aging. *PLoS ONE* **7**, e44457 (2012).

73. Suopanki, J. *et al.* Interaction of huntingtin fragments with brain membranes - clues to early dysfunction in Huntington's disease. *J Neurochem* **96**, 870–884 (2006).
74. Leitman, J., Ulrich Hartl, F. & Lederkremer, G. Z. Soluble forms of polyQ-expanded huntingtin rather than large aggregates cause endoplasmic reticulum stress. *Nat Commun* **4**, 2753 (2013).
75. Drombosky, K. W. *et al.* Mutational analysis implicates the amyloid fibril as the toxic entity in Huntington's disease. *Neurobiology of Disease* **120**, 126–138 (2018).
76. Weber, J. J., Sowa, A. S., Binder, T. & Hübener, J. From Pathways to Targets: Understanding the Mechanisms behind Polyglutamine Disease. *BioMed Research International* **2014**, 1–22 (2014).
77. Jayaraman, M. *et al.* Slow Amyloid Nucleation via α-Helix-Rich Oligomeric Intermediates in Short Polyglutamine-Containing Huntingtin Fragments. *Journal of Molecular Biology* **415**, 881–899 (2012).
78. Altschuler, E. L., Hud, N. V., Mazrimas, J. A. & Rupp, B. Random coil conformation for extended polyglutamine stretches in aqueous soluble monomeric peptides. *The Journal of Peptide Research* **50**, 73–75 (2009).
79. Lakhani, V. V., Ding, F. & Dokholyan, N. V. Polyglutamine Induced Misfolding of Huntingtin Exon1 is Modulated by the Flanking Sequences. *PLoS Comput Biol* **6**, e1000772 (2010).
80. Bhattacharyya, A. *et al.* Oligoproline Effects on Polyglutamine Conformation and Aggregation. *Journal of Molecular Biology* **355**, 524–535 (2006).
81. Darnell, G., Orgel, J. P. R. O., Pahl, R. & Meredith, S. C. Flanking Polyproline Sequences Inhibit β-Sheet Structure in Polyglutamine Segments by Inducing PPII-like Helix Structure. *Journal of Molecular Biology* **374**, 688–704 (2007).
82. Darnell, G. D., Derryberry, J., Kurutz, J. W. & Meredith, S. C. Mechanism of Cis-Inhibition of PolyQ Fibrillation by PolyP: PPII Oligomers and the Hydrophobic Effect. *Biophysical Journal* **97**, 2295–2305 (2009).
83. Hoop, C. L. *et al.* Polyglutamine Amyloid Core Boundaries and Flanking Domain Dynamics in Huntingtin Fragment Fibrils Determined by Solid-State Nuclear Magnetic Resonance. *Biochemistry* **53**, 6653–6666 (2014).
84. Crick, S. L., Ruff, K. M., Garai, K., Frieden, C. & Pappu, R. V. Unmasking the roles of N- and C-terminal flanking sequences from exon 1 of huntingtin as modulators of polyglutamine aggregation. *Proc. Natl. Acad. Sci. U.S.A.* **110**, 20075–20080 (2013).
85. Sivanandam, V. N. *et al.* The Aggregation-Enhancing Huntingtin N-Terminus Is Helical in Amyloid Fibrils. *J. Am. Chem. Soc.* **133**, 4558–4566 (2011).
86. Burke, K. A., Hensal, K. M., Umbaugh, C. S., Chaibva, M. & Legleiter, J. Huntingtin disrupts lipid bilayers in a polyQ-length dependent manner. *Biochimica et Biophysica Acta (BBA) - Biomembranes* **1828**, 1953–1961 (2013).
87. Mishra, R. *et al.* Inhibiting the Nucleation of Amyloid Structure in a Huntingtin Fragment by Targeting α-Helix-Rich Oligomeric Intermediates. *Journal of Molecular Biology* **415**, 900–917 (2012).
88. Atwal, R. S. *et al.* Huntingtin has a membrane association signal that can modulate huntingtin aggregation, nuclear entry and toxicity. *Human Molecular Genetics* **16**, 2600–2615 (2007).
89. Burke, K. A., Godbey, J. & Legleiter, J. Assessing mutant huntingtin fragment and polyglutamine aggregation by atomic force microscopy. *Methods* **53**, 275–284 (2011).

90. Kelley, N. W. *et al.* The Predicted Structure of the Headpiece of the Huntingtin Protein and Its Implications on Huntingtin Aggregation. *Journal of Molecular Biology* **388**, 919–927 (2009).
91. Williamson, T. E., Vitalis, A., Crick, S. L. & Pappu, R. V. Modulation of Polyglutamine Conformations and Dimer Formation by the N-Terminus of Huntingtin. *Journal of Molecular Biology* **396**, 1295–1309 (2010).
92. Monsellier, E., Redeker, V., Ruiz-Arlandis, G., Bousset, L. & Melki, R. Molecular Interaction between the Chaperone Hsc70 and the N-terminal Flank of Huntingtin Exon 1 Modulates Aggregation. *Journal of Biological Chemistry* **290**, 2560–2576 (2015).
93. Thakur, A. K. *et al.* Polyglutamine disruption of the huntingtin exon 1 N terminus triggers a complex aggregation mechanism. *Nat Struct Mol Biol* **16**, 380–389 (2009).
94. Vieweg, S. *et al.* The Nt17 Domain and its Helical Conformation Regulate the Aggregation, Cellular Properties and Neurotoxicity of Mutant Huntingtin Exon 1. *Journal of Molecular Biology* **433**, 167222 (2021).
95. Ueda, M. *et al.* Expanded polyglutamine embedded in the endoplasmic reticulum causes membrane distortion and coincides with Bax insertion. *Biochemical and Biophysical Research Communications* **474**, 259–263 (2016).
96. Kegel, K. B. *et al.* Huntingtin Associates with Acidic Phospholipids at the Plasma Membrane. *Journal of Biological Chemistry* **280**, 36464–36473 (2005).
97. Yan, S. *et al.* A Huntingtin Knockin Pig Model Recapitulates Features of Selective Neurodegeneration in Huntington's Disease. *Cell* **173**, 989-1002.e13 (2018).
98. Song, W. *et al.* Mutant huntingtin binds the mitochondrial fission GTPase dynamin-related protein-1 and increases its enzymatic activity. *Nat Med* **17**, 377–382 (2011).
99. Bäuerlein, F. J. B. *et al.* In Situ Architecture and Cellular Interactions of PolyQ Inclusions. *Cell* **171**, 179-187.e10 (2017).
100. Qin, Z.-H. Huntingtin Bodies Sequester Vesicle-Associated Proteins by a Polyproline-Dependent Interaction. *Journal of Neuroscience* **24**, 269–281 (2004).
101. Harjes, P. & Wanker, E. E. The hunt for huntingtin function: interaction partners tell many different stories. *Trends in Biochemical Sciences* **28**, 425–433 (2003).
102. Michalek, M., Salnikov, E. S., Werten, S. & Bechinger, B. Membrane Interactions of the Amphipathic Amino Terminus of Huntingtin. *Biochemistry* **52**, 847–858 (2013).
103. Burke, K. A., Kauffman, K. J., Umbaugh, C. S., Frey, S. L. & Legleiter, J. The Interaction of Polyglutamine Peptides with Lipid Membranes Is Regulated by Flanking Sequences Associated with Huntingtin. *Journal of Biological Chemistry* **288**, 14993–15005 (2013).
104. Michalek, M., Salnikov, E. S. & Bechinger, B. Structure and Topology of the Huntingtin 1–17 Membrane Anchor by a Combined Solution and Solid-State NMR Approach. *Biophysical Journal* **105**, 699–710 (2013).
105. Côté, S., Wei, G. & Mousseau, N. Atomistic mechanisms of huntingtin N-terminal fragment insertion on a phospholipid bilayer revealed by molecular dynamics simulations: htt $^{NT}Q_{N}$ Insertion on a Phospholipid Bilayer. *Proteins* **82**, 1409–1427 (2014).
106. Burke, K. A., Yates, E. A. & Legleiter, J. Amyloid-Forming Proteins Alter the Local Mechanical Properties of Lipid Membranes. *Biochemistry* **52**, 808–817 (2013).

107. Bernstein Sideman, A. *et al.* Facilitators and Barriers to Dementia Assessment and Diagnosis: Perspectives From Dementia Experts Within a Global Health Context. *Front. Neurol.* **13**, 769360 (2022).
108. Alzheimer's Association. 2022 Alzheimer's Disease Facts and Figures.
109. for the SCarlet RoAD Investigators *et al.* A phase III randomized trial of gantenerumab in prodromal Alzheimer's disease. *Alz Res Therapy* **9**, 95 (2017).

Chapter 2 Blocking the ability of huntingtin to bind membranes: a therapeutic strategy for Huntington's disease

2.1 Introduction

The aggregation of proteins into amyloid deposits is a hallmark of many neurodegenerative diseases including Alzheimer's disease (AD), Parkinson's disease (PD), and Huntington's disease (HD)[1]. The formation of amyloid fibrils is complex and includes a variety of intermediate oligomers and protofibrils. Many of these different aggregate forms are linked to toxic gains of function, leading to immense effort to develop therapeutic strategies that inhibit or manipulate amyloid formation[2]. However, this approach has had limited success in leading to the development of efficacious drugs. Many amyloid-forming proteins and their aggregates directly bind and damage lipid membranes[3]. For example, high molecular weight oligomers of β-amyloid (Aβ) associated with AD disturb plasma membrane integrity, resulting in decreased membrane fluidity, intracellular calcium dysregulation, depolarization and impaired long-term potentiation[4]. α-synuclein (α-syn) interacts with multiple organelle membranes causing defects in mitochondrial function and membrane trafficking in PD[5,6]. This suggests that blocking the interaction between disease-related proteins (and their aggregate forms) and (sub)cellular membranes is a viable target for therapeutic intervention.

HD is a genetic neurodegenerative disease that is caused by the abnormal expansion of a polyglutamine (polyQ) tract near the N -terminus of the huntingtin protein (htt). PolyQ expansion beyond a critical threshold (~35 repeats) results in HD. Like other amyloids, htt strongly interacts with various membranous surfaces, and a variety of membrane abnormalities are associated with the presence of mutant htt. Inclusions of htt damage and distort the nuclear envelope in a manner associated with cell death[7]. Furthermore, mutant htt exasperates age-dependent disruption of the nuclear envelope, invoking DNA damage[8]. Htt fibrils impinge on cellular endomembranes, damaging their integrity and freezing ER dynamics[9]. In mammalian cell and primary neuron models of HD, cytoplasmic htt inclusions contain remnants of organelle membranes from the ER and mitochondria, which correlates with impaired organelle function and localization[10].

Damaged organelle membranes (swollen mitochondria and absent nuclear membrane) are also observed in a novel pig model of HD[11].

Directly preceding the polyQ domain are the first 17 N-terminal amino acids (Nt17, MATLEKLMKAFESLKSF) of htt that acts as a lipid-binding domain[12,13]. In bulk solution, Nt17 is intrinsically disordered but forms an amphipathic α-helix (AH) to facilitate membrane binding[13]. Beyond its role in lipid-binding, Nt17 forms intermolecular associations to form α-helical rich oligomers that promote nucleation of fibril formation[14,15]. This dual role of Nt17 in lipid binding and aggregation is underscored by the direct influence of lipid membranes on the kinetics and mechanism of htt aggregation[14]. This impact of membranes on htt aggregation is highly dependent on lipid composition. For example, total brain lipid extract (TBLE) stabilizes oligomers of truncated polyQ peptides that contain Nt17[12] and impedes fibrillization of htt-exon1[16]. In contrast, POPC/POPS lipid vesicles enhance aggregation via a unique Nt17-mediated mechanism involving membrane anchoring and two-dimensional diffusion[14]. In general, anionic headgroups accelerate fibril formation[17] and there is a complementarity relationship between hydrophobic residues and membrane defects, regulating the partitioning of Nt17 into bilayers[18]. The ability of htt to bind membranes is also dependent on aggregation state, with oligomers having the strongest affinity for lipid vesicles in comparison to monomers and fibrils[19].

To determine if blocking the ability of amyloid-forming proteins to bind membranes would have potential therapeutic benefit, the interaction of mutant htt with membranes was used as a model system. A systematic screen was performed to identify compounds that block the binding of htt oligomers to lipid vesicles comprised of TBLE. After validation by additional methods, two compounds were identified. The impact of these compounds on htt aggregation and the mechanism by which these compounds block the htt/lipid interaction were then determined. Finally, the ability of these compounds to improve phenotype in a *C. elegans* model of HD was demonstrated. Collectively, our work demonstrates the proof of principle that blocking the binding of amyloid-forming proteins to membranes is a viable therapeutic strategy and provides a method for compound identification and validation.

2.2 Methods

2.2.1 Purification of GST-htt-exon1 fusion protein

Glutathione *S*-transferase (GST)-htt-exon1 fusion protein with 46 glutamine repeat units was purified as described previously[20]. In brief, GST-htt exon 1 (htt) was expressed in *Escherichia coli* by induction with isopropyl β-D- thiogalactoside at 30 °C for 4 h. Cells were lysed with a combination of lysozymes (0.5mg/mL) and probe sonication. The protein was purified from the lysate with a GST affinity column using LPLC, Bio-rad liquid chromatography. Relevant fractions were identified using ultraviolet absorption and confirmed by gel electrophoresis. The protein was subjected to dialysis for 48 h. Before use in any assay, the protein was centrifuged for 30 min at 20000 ×g at 4 °C to remove preexisting fibrils. Factor Xa (New England Biolabs) was used to cleave the GST tag. All experiments were carried out in a buffer composed of 50 mM Tris-HCl, 150 mM NaCl.

2.2.2 TBLE/PDA assay.

TBLE/PDA assays were performed as reported previously[21]. Shortly, TBLE (Avanti lipids) and 10,12 tricosadiynoic acid were combined in a molar ratio of 2:3 in an ethanol/chloroform mixture. Solutions were dried under a stream of N_2 for 15 min. The resulting film was re-suspended in 50 mM tris buffered saline at 70 °C. After 5 min of probe sonication, solutions were stored at 4 °C overnight to allow self-assembly of vesicles. The diacetylene monomers were polymerized by irradiation under 254 nm for 15 min, resulting in a bright blue color solution. Prior to use in TBLE/PDA assay, htt-exon1(46Q) was incubated on ice with Factor Xa for 90 minutes to allow cleavage and formation of oligomers. Final concentration of htt-exon1(46Q) in TBLE/PDA assays was 10 µM.

For TBLE/PDA screening assays, the LOPAC 1280 library was used in a 96 well plate format, with each plate screening 80 compounds. Polymerized PDA/TBLE vesicles were added to all the wells in the plate excluding column 12. Column 1 was reserved for controls. As a negative control, 50 mM tris saline buffer was added to cells A1, B1, and C1. Wells D1, E1, and F1 were exposed to htt-exon1(46Q). As a positive control, saturated NaOH was added to wells G1 and H1 to ensure PDA/TBLE vesicles were

working properly. A unique compound was added to wells in columns 2-11 at a final concentration of 100 µM, along with 10 µM htt-exon1 making the final compound to htt ratio 10:1 in the screening assays. Plates were incubated at 25 °C and colorimetric response (CR) was determined at 1 h, 3 h, and 5 h by measuring the blue absorbance (640 nm, A_{blue}) and the red absorbance (500 nm, A_{red}) (Spectramax M2) and using:

$$CR = \frac{PB_0 - PB_1}{PB_0} \qquad (1)$$

where PB is defined as $A_{blue}/(A_{blue} + A_{red})$. PB_0 is determined from the negative control, and PB_1 is obtained from each experimental condition.

For PDA/TBLE kinetic assays, polymerized PDA/TBLE vesicles were exposed to htt-exon1 (46Q) at a final concentration of 10 µM in the presence of either Ro90-7501 or Benzamil (TOCRIS) at various ratios. 50 mM tris saline buffer was used as the negative control. CR was determined every 5 min for 15 h. All experiments were carried out in 96-well plates at 25 °C.

2.2.3 Calcein dye leakage assay

Large unilamellar vesicles (LUVs) of POPC with entrapped calcein were prepared as described[22]. Lipid films were suspended in calcein buffer (70 mM calcein 10 mM Tris, 150 mM NaCl pH 7.4). To promote LUV formation, the lipid solutions were subjected to 10 freeze-thaw cycles followed by bath sonication for 30 min. Excess dye was removed with size exclusion chromatography using Sephadex G-50 beads (Sigma-Aldrich) using 10 mM Tris, 150 mM NaCl as the eluent. Vesicles were exposed to 10 µM htt-exon1(46Q) in the absence and presence of Ro (1x) and Benzamil (2x). Calcein fluorescence was measured at 515nm (495 nm excitation) prior to the addition of protein and 10 min after the addition of protein at 37 °C. Vesicles were then lysed with 1% Triton X-100 to obtain maximum fluorescence. Relative leakage was calculated by

$$Relative\ leakage = \frac{I_f - I_i}{I_t - I_i} \qquad (2)$$

where I_f is the fluorescent intensity after addition of protein, I_i is the fluorescent intensity before addition of protein, and I_t is the fluorescent intensity after lysis.

2.2.4 Atomic force microscopy (AFM)

All AFM imaging was performed with a Nanoscope V Multimode atomic force microscope (Veeco, Santa Barbara, CA) equipped with a closed-loop vertical engage J-scanner. For *ex situ* AFM experiments to determine the impact of compounds on aggregation, htt-exon1(46Q) (10µM) was incubated in the absence and presence of Ro or Benzamil at 37 ˚C and sampled after 1 h, 3 h, 5 h and 8h for imaging. At each time point, a 5 µL aliquot of each sample was deposited on freshly cleaved mica, allowed to set for 1 min, washed with ultrapure water, and dried with a stream of air. Imaging was done using silicon oxide cantilevers with a normal spring constant of ~40 N/m and resonance frequency of ~300 kHz at a scan rate of ~2Hz.

For *in situ* AFM imaging of htt-exon1(46Q) occurring directly on lipid bilayers, silicon nitride cantilevers with a spring constant of ~0.1 N/m were used. 25 µL aliquots of TBLE vesicles were injected directly into the fluid cell at a concentration of 1 mg/mL. The formation of a continuous defect free bilayer on mica via vesicle fusion was observed by continual AFM imaging. Htt-exon1(46Q) that had been incubated at 4 °C for 90 min with factor Xa was injected into the fluid cell to a final concentration of 10 µM. For experiments with either Ro (2x) or Benzamil (1x), the drug was incubated with the htt-exon1(46Q) prior to injection into the fluid cell. Images obtained by both *ex situ* and *in situ* AFM were processed and analyzed using MATLAB as described previously[23].

2.2.5 Thioflavin T (ThT) assay

ThT assays were conducted in 96- well plates on a Spectramax M2 microplate reader (Molecular Devices). Final ThT concentration in each well was 40 µg/mL. The aggregation of htt in the presence of varying doses of Ro or Benzamil was investigated by measuring ThT fluorescence at 484 nm emission (440 nm excitation) at 37 °C for 15 h with readings taken every 10 min. All experimental conditions were performed in triplicates. For analysis

of Ro's ability to compete with ThT to bind fibrils, htt-exon1(46Q) was incubated at 37 °C for 24 h to obtain a predominately fibrillar sample. Fibrils were then incubated with either ThT or ThT with Ro ensuring a final htt:Ro ratio of 1:1 at 37 °C for 1 h and ThT fluorescence was measured.

2.2.6 Molecular dynamic (MD) simulations

A Nt17 tetramer structure by Kotler et al (6N8C) was utilized to perform MD simulation[24]. For monomer simulations one peptide from the tetramer structure was extracted. Initially the peptides were solvated in water (TIP3) and neutralized with NaCl (150 mM) using Charmm-gui[25] and was subjected to energy minimization and equilibration. Ro and Benzamil were then introduced to the equilibrated peptide structures using packmol[26]. For monomer and tetramer simulations, three and ten drug molecules were added respectively. The resulting structures (peptide + drug) were then solvated and ionized to a final NaCl concentration of 150 mM using VMD solvate and ionize plugins[27]. Ro and Benzamil were parameterized with CHARMM General Force Field (CGenFF)[28]. Nano-scale molecular dynamics (NAMD 2.14)[29] was used to perform all simulations on CHARMMc36 force field[28]. The temperature and pressure parameters were set to 310 K and 1.01325 bar respectively. All atom simulations were carried out for 300 ns with a 2 fs timestep after minimizing and equilibrating for 20 ns. Each simulation was carried in triplicate. Trajectories were analyzed using VMD[27] and MATLAB.

2.2.7 C.elegans

Two *C.elegans* strains EAK 102 expressing htt-513(Q15) and EAK 103 expressing htt-513(Q128)[30] were obtained from Caenorhabditis Genetics Center. Worms were maintained at 20 °C in NGM plates inoculated with OP50 under standard techniques. Age synchronized worms were obtained using previously described methods[31]. EAK 102 (Q15) serves only as a control in all experiments while EAK 103 (Q128) was treated with either Ro or Benzamil.

Survival assays were performed in 96 well plates. The culture medium was prepared as described previously[31]. Final OP50 concentration in the well was set to 0.05 mg/mL. Fluorodeoxyuridine (FUdR) was used to prevent the synchronous population from

reproducing[32] and the final FUdR concentration was set to 400 µM. Ro or Benzamil were added to the culture medium to obtain desired final concentration. For each well ~ 10 age synchronized L4 worms were introduced. Viability of the animals was determined every other day for up to 25 days, animals that do not move upon shaking for 30 s on a plate shaker were scored as deceased. Each condition was tested for a minimum of 50 animals per trial.

For thrashing assays, drug induced NGM plates (35 mm diameter) were prepared with a final FUdR concentration of 400 µM. For each plate ~100 age synchronized L4 worms were introduced and were maintained at 20 °C. Thrashing rate was observed on day 2 and 7 of the adulthood. Animals were picked from plates in 25 µL drops of M9 buffer and placed on a microscopic slide. They were given 30 s recovery time, and a 1 min video of their thrashing in liquid was recorded. The videos were processed and analyzed using MATLAB image processing toolbox and Image J equipped with worm tracker plugin[33,34]. A minimum of 35 animals were assessed for each condition per trial.

To measure inclusion formation via fluorescent microscopy, adult day 7 animals were obtained from NGM plates and were suspended in 15 mg/ mL 2,3-Butanedione monoxime (BDM) for 30-60 mins to induce paralysis in worms. Once paralyzed the worms were imaged in solution with either 10x magnification or 20x magnification. Inclusion counts in each image was determined by counting the fluorescent foci in each worm.

2.3 Results

2.3.1 Identifying compounds that block htt/lipid binding

To determine if blocking the ability of htt to bind membranes has therapeutic potential, identification of molecules that directly interfere with the binding process was required. To accomplish this, polydiacetylene (PDA)/TBLE lipid binding assays were used to screen the LOPAC1280 library (Figure 2.1a). As protein binds to PDA/TBLE vesicles, the associated mechanical stress on the PDA component causes a quantifiable colorimetric response (CR) from blue to red. As htt oligomers have the highest affinity for

lipid membranes[19], PDA/TBLE vesicles were exposed to pre-aggregated, oligomeric htt-exon1(46Q) (10 μM), and the dose of each screened compound was 10x that of htt. As designed, the assay only identified molecules that block htt/lipid interactions by targeting the protein, as compounds that directly associate with PDA vesicles invoke a CR[16]. After 5 h of exposure to htt oligomers, compounds that reduced the CR to 20% of the control response (htt alone) were considered potential hits (Figure 2.1b). After the initial screen, hits were re-tested in triplicate, and two promising compounds were identified, Ro90-7501 (Ro) and Benzamil (Ben). Ro is a known inhibitor of Aβ and α-syn fibrillization[35,36]. Ben is a potent blocker of the ENaC channel[37] and a sodium-calcium exchange blocker[38].

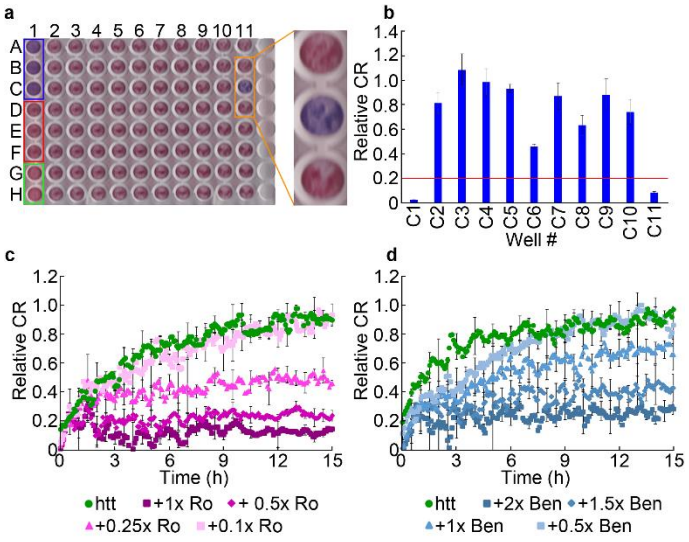

Figure 2.1 Screen for compounds that inhibit htt binding to lipid membranes. a, Representative 96-well plate used for the PDA/TBLE assay after 5 h of exposure to htt-exon146Q. Blue box indicates wells in which vesicles were exposed to neat buffer (negative control). Red box indicates control wells in which vesicles exposed to htt-exon1(46Q). Green box indicated wells in which vesicles were exposed to NaOH (positive control). Inset (indicated by yellow box) highlights wells in which the screened compounds did not inhibit binding to vesicles (top and bottom wells) and a well in which the screened compound did (middle well). **b,** Relative colorimetric response of PDA/TBLE vesicles measured from row C of the plate shown in a. Red line represents the hit threshold. The data is normalized with respect to the htt-exon1(46Q) controls. **c** and **d,** Relative colorimetric response of PDA/TBLE vesicles exposed to htt-exon1 (10 μM) measured kinetically in the presence of varying doses of Ro and Ben normalized with respect to htt control. All error bars represent SEM.

To determine appropriate dosing of each drug for additional validation and experimentation, a series of kinetic PDA/TBLE assays were performed in which the dose

of each compound was systematically lowered, and the assay time was extended to 15 h (Figure 2.1c-d). Ro continued to reduce the relative CR below 0.2 with doses as low as 0.5x that of htt. After that, the effectiveness of Ro decreases in a dose-dependent manner until non-significant reduction in relative CR was observed at 0.1x Ro. For Ben, higher doses were needed to suppress vesicle binding. While the 2x dose of Ben reduced the relative CR to ~ 0.2, a dose of 0.5x Ben no longer provided a statistically significant reduction.

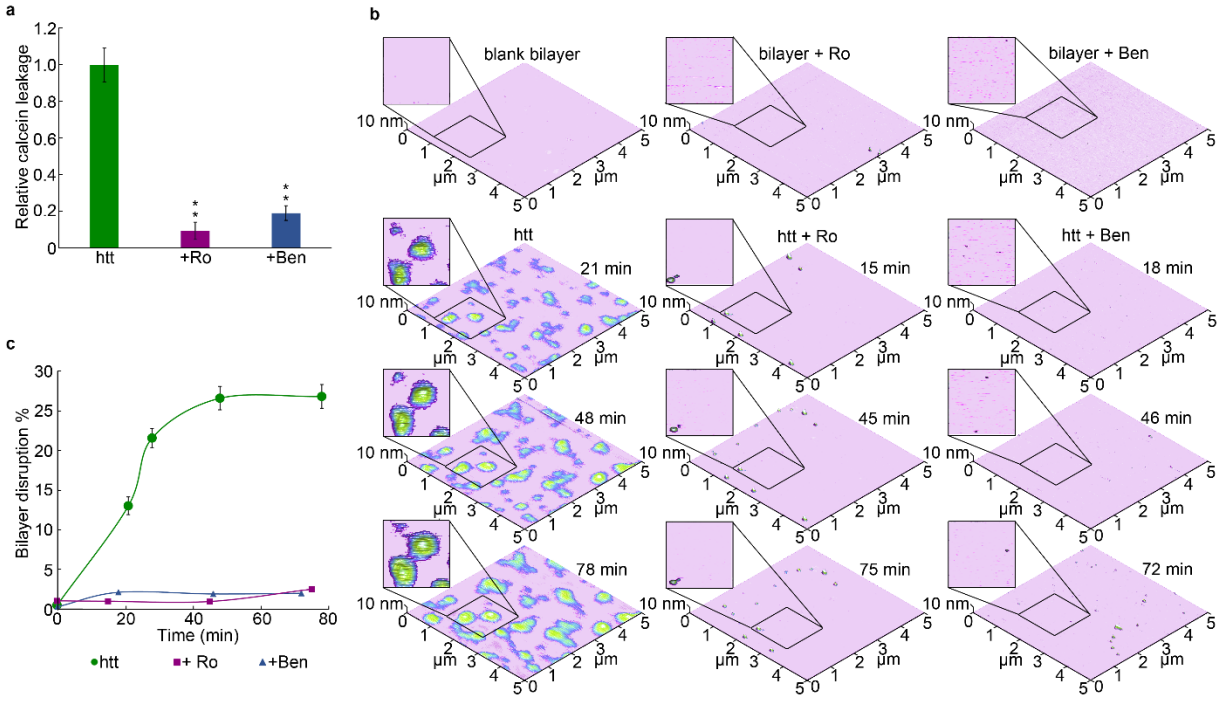

Figure 2.2 Validation that Ro and Ben inhibit htt binding to lipid membranes. a, Calcein dye leakage assay from POPC vesicles exposed to htt-exon1(46Q) (10 μM). Dosing of Ro and Ben were1x and 2x the htt concentration respectively. The data was normalized with respect to htt control. **b,** In situ AFM images of supported TBLE bilayers exposed to htt-exon1(46Q) (10μM) or htt-exon1(46Q) incubated with either 1x Ro or 2x Ben **c,** The % area of the bilayer disrupted by exposure to htt-exon1(46Q) determined from in situ AFM images. All error bars represent SEM and * indicates P<0.01.

To further validate that the compounds blocked htt/lipid binding, additional assays were performed (Figure 2.2). First, a calcein dye leakage assay (using POPC vesicles)

was performed with effective doses established by the kinetic PDA assays (Figure 2.2a). Both compounds significantly suppressed dye leakage ($p<0.01$). With a 1x dose of Ro, the fluorescent signal associated with the dye leakage was reduced to 0.1 relative to the leakage caused by htt. A 2x dose of Ben reduced the leakage to less than 0.2. Next, the impact of htt exposure on supported TBLE bilayer morphology was directly monitored by in solution AFM (Figure 2.2b). Supported bilayers were formed on mica via vesicle fusion. These bilayers are stable for several hours and have a smooth appearance with an RMS roughness < 0.2 nm. Upon exposure to 10 μM htt oligomers, regions of roughened morphology (RMS of 0.6-1.2 nm) developed on the bilayer surfaces, and the area of membrane disruption grew with time until ~25% of the bilayer area is altered (Figure2.2b-c). When either 10 μM Ro (1x) or 20 μM Ben (2x) was added prior to exposure to htt oligomers, bilayer morphology was relatively unaffected (< 5% of the bilayer area) except for the appearance of a few discrete aggregate structures (Figure 2.2b-c). Collectively, the PDA, calcein dye, and AFM assays validate that Ro and Ben reduce the ability of htt to bind and damage lipid membranes.

2.3.2 Impact of Ro and Ben on htt aggregation

As the initial screens were designed to identify compounds that directly interact with htt, it is plausible that Ro and Ben could impact htt aggregation directly. To initially determine if Ro and Ben modify fibril formation, ThT assays were performed using doses of the compounds that effectively inhibited membrane binding. Ro reduced the ThT signal associated with 10 μM htt aggregation in a dose-dependent manner (Figure 2.3a). However, due to Ro being structurally similar to ThT, there is a possibility that it competes with ThT binding sites on htt fibrils, resulting in reduced ThT signal without inhibiting

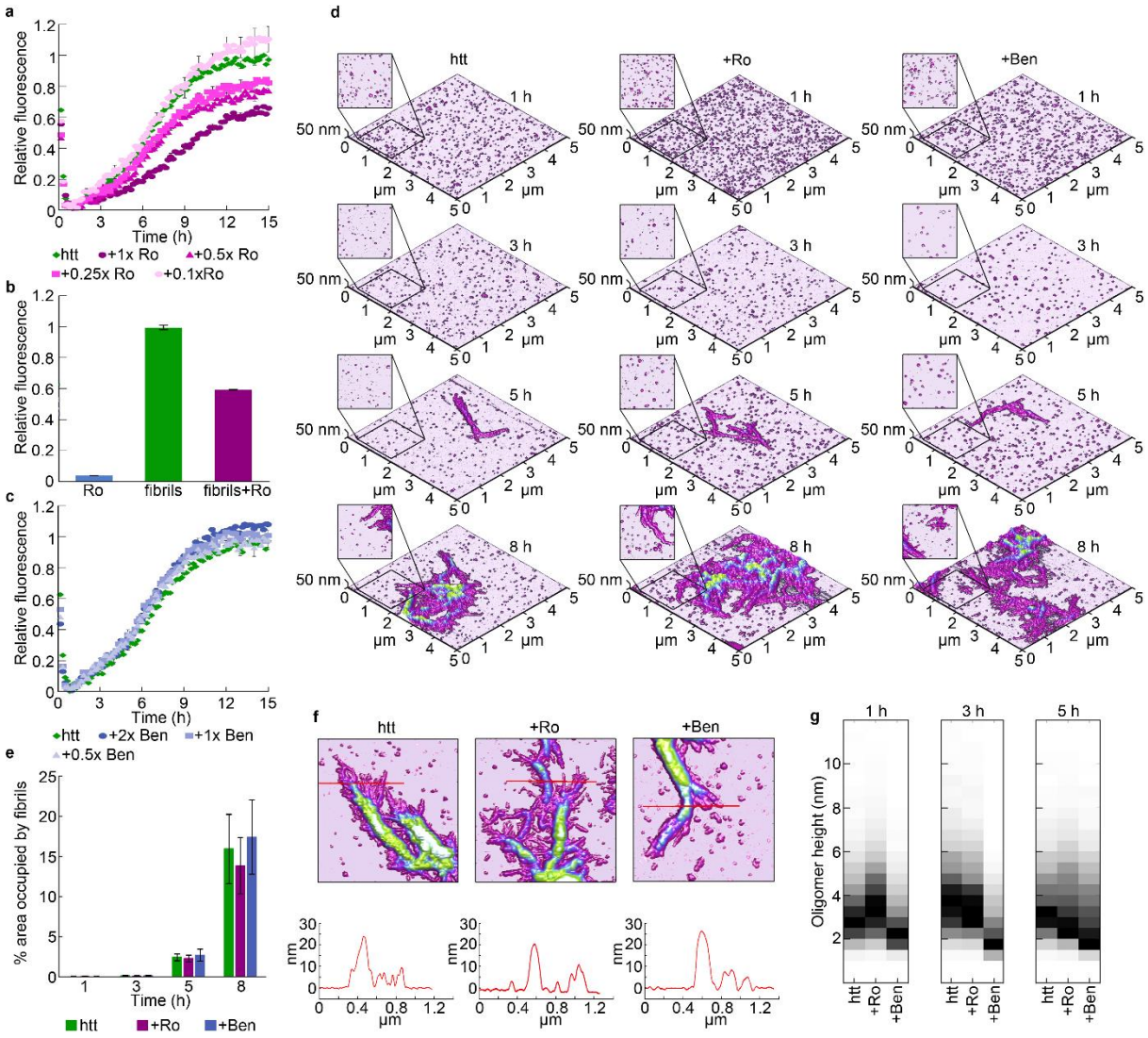

Figure 2.3 Impact of Ro and Ben on htt aggregation. a, ThT fluorescence assay of htt-exon1(46Q) (10 μM) with varying doses of Ro normalized to the htt control. **b,** Relative ThT fluorescence of pre-formed htt-exon1(46Q) fibrils (10 μM) incubated with ThT and ThT +1x Ro. Ro fluorescence without fibrils was used as a control. Signals were normalized to ThT fluorescence of htt fibrils alone. **c,** ThT fluorescence assay of htt-exon1(46Q) (10 μM) exposed to varying doses of Ben normalized with respect to the htt control. **d,** Representative ex situ AFM images of htt-exon1(46Q) (10 μM) incubated alone and with 1x Ro or 2x Ben and deposited on mica at various timepoints. **e**, The surface area covered by fibrils calculated from AFM images. **f,** Comparison of fibrils formed in the absence or presence of either 1x Ro or 2x Ben. Red lines in the images correspond to the height profiles directly below the image. **h,** Height histograms of all oligomers formed by htt-exon1(46Q) in the absence or presence of either 1x Ro or 2x Ben as function of time, each column is normalized by dividing the entire distribution by the number of oligomers contained in the most populated bin. All error bars represent SEM.

aggregation. Therefore, htt was pre-aggregated to obtain solutions predominately comprised of fibrils. These solutions were exposed to ThT or a combination of ThT and Ro at the same ratios as the kinetic ThT assays, and the resulting ThT fluorescence was measured (Figure 2.3b). The ThT signal was reduced in the presence of Ro to comparable levels as observed in the kinetic assays (~35-40% reduction with 1x Ro). Based on the absorption spectra of Ro (Figure 2.4), it does not interfere with the ThT excitation or emissions signals either. This suggests that Ro competitively bound fibrils and does not suppress htt fibril formation. Ben did not modify fibril formation based on the ThT assay with doses as high as 2x (Figure 2.3c).

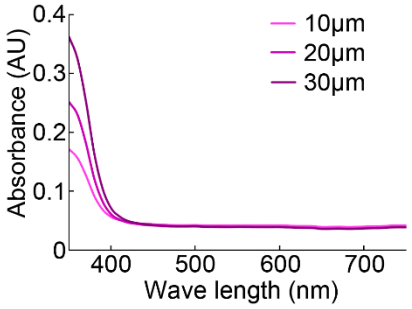

Figure 2.4 Absorbance spectrum of RO at different concentrations.

In addition to the competitive binding of Ro, ThT assays do not provide direct information on potential changes in fibril morphology or oligomer formation. To identify whether Ro and Ben alter morphology of htt aggregates, incubations of 10 µM htt alone, with 1x Ro, or 2x Ben were sampled at several time points and evaluated using *ex situ* AFM (Figure 2.3d). For all three conditions, only oligomers were observed after 1 and 3 h of incubation, and fibrils emerged after 5 h. At 8 h, all conditions exhibited extensive fibril formation and bundling. Based on the surface area occupied by fibrils at each timepoint, neither compound inhibited fibril formation (Figure 2.3e), consistent with the ThT assays when taking into account the competitive binding of Ro for htt fibrils. Additionally, fibril morphology was unaltered by the presence of either Ro or Ben, as single fibril strands were typically 7-9

nm thick (Figure 2.3f). Fibril bundles were also similar in thickness. To characterize oligomer morphology additional image analysis was performed using automated algorithms that measure morphological features of all aggregates present in an AFM image (Figure 2.3g). In this analysis, oligomers were defined as objects greater than 0.8 nm in height and with an aspect ratio less than 2.5 (globular structure) and occupying a surface area < 0.008 μm^2. After 1, 3, and 5 h of incubation, oligomers formed by htt alone or with Ro were similar in size (mode height ~2.5-4 nm,); however, the addition of Ben resulted in systematically smaller oligomers (mode height ~1.5 – 2.5 nm), suggesting that Ben altered oligomer structure without reducing their efficiency in nucleating fibrilization.

2.3.3 Mechanism of interaction of Ro and Ben with htt

As Nt17 facilitates the interaction of htt-exon1 with lipid membranes[12,13], it is likely that Ro and Ben directly interact with Nt17. To gain insight into this potential interaction, molecular dynamics (MD) simulations were performed with both monomeric and oligomeric forms of Nt17 exposed to each compound (Figures 2.5-2.10). For the oligomer structure, the tetramer of Nt17 resolved by Kotler et al was used[24]. This structure is a dimer of dimers having anti-parallel Nt17 helical units. It is important to point out that oligomers observed by AFM in this study are typically larger than tetramers; however, this NMR structure is the only one currently available. For the monomeric simulations, a single Nt17 peptide from the tetramer structure was used and was therefore initially α-helical. The NMR structure was determined from peptides lacking the first methionine residue of Nt17 because this residue is typically cleaved off *in vivo*. For ease of comparison later with htt-exon1 experiments, the amino acids are numbered here with the missing methionine being considered the first residue.

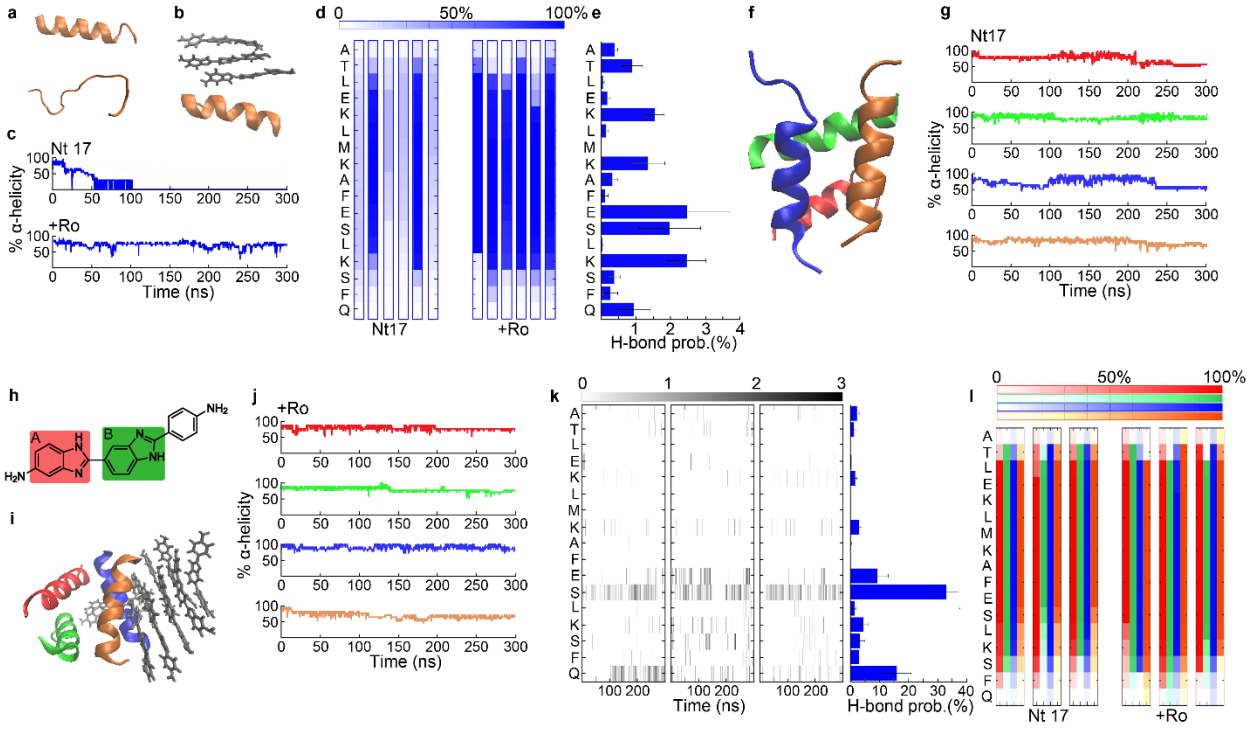

Figure 2.5 MD simulations of the interaction of Ro with Nt17. **a,** The initial Nt17 monomer structure and after 150 ns of simulation. **b,** Nt17 monomer interacting with Ro molecules after 150 ns of simulation. **c,** The percent α-helicity of Nt17 monomer in the presence and absence of Ro as a function of time (five additional simulations provided in Figure 2.6). **d,** The average percent α-helicity of each residue in Nt17 monomers in the absence and presence of Ro. For each condition, the individual heat maps represent an independent simulation. **e,** Residue specific, hydrogen bonding probability density of Ro with Nt17 monomer averaged across six independent simulations. **f,** Nt17 tetramer structure after 150 ns of simulation. **g,** The percent α-helicity of each Nt17 peptide within the tetramer structure as a function of time (two additional simulations provided in Figure 2.7). **h,** Structure of Ro with each benzimidazole highlighted. **i**, Nt17 tetramer structure exposed to Ro molecules after 150 ns of simulation. **j,** The percent α-helicity of each Nt17 peptide within the tetramer structure upon exposure to Ro as a function of time (three additional simulations provided in Figure 2.7). **k,** Residue specific, time-dependent hydrogen bonding profile and probability density of Ro with the Nt17 tetramer. Each heat map represents an independent simulation. **l**, The average percent α-helicity of each residue in Nt17 broken down by peptide within the tetramer structure in the absence or presence of Ro. Three independent simulations are shown for each condition. Each column consists of 4 heat-maps representing the different Nt17 peptides (color coded). All error bars represent SEM.

While the initial structure of the Nt17 monomer was helical, this secondary structure was unstable in the absence of any compounds and became completely

disordered within 50-100 ns in four out of six simulations (Figure 2.5a-c and Figure 2.6a). Even in the simulations in which helical structure was present for the vast majority of the simulation time, there were several instances in which the Nt17 completely unfolded and refolded (Figure 2.6a). Addition of three Ro molecules stabilized the α-helical structure of Nt17 (Figure 2.5b-d and Figure 2.6b). Comparison of the α-helical probability of each residue in Nt17 in the absence and presence of Ro across each simulation demonstrates a clear stabilization of the helical structure (Figure 2.5d). While Ro would intermittently form H-bonds with most residues of Nt17 (M8 being an exception), these H-bonds were short-lived (typically in the range of 0.3±0.1 ns and occurring less than 5% of the total simulation time for any given residue (Figure 2.5e). Ro-907501 had a slight preference for interaction with the adjacent residues E12 and S13, as well as K15 (Figure 2.5e). Binding of additional Ro molecules to an Nt17-Ro complex was facilitated by extensive π-stacking upon the bound Ro molecule.

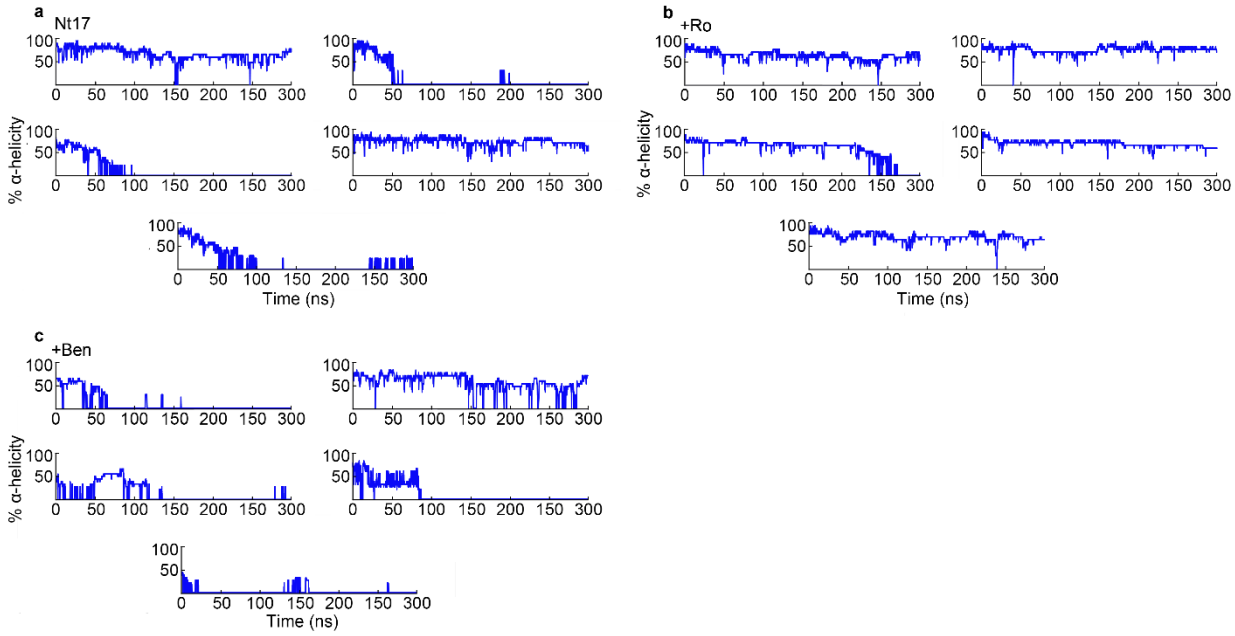

Figure 2.6 Percentage alpha helicity of a, Nt17 monomer and **b**, Nt17 monomer +Ro or **c**, +Ben for five additional simulations.

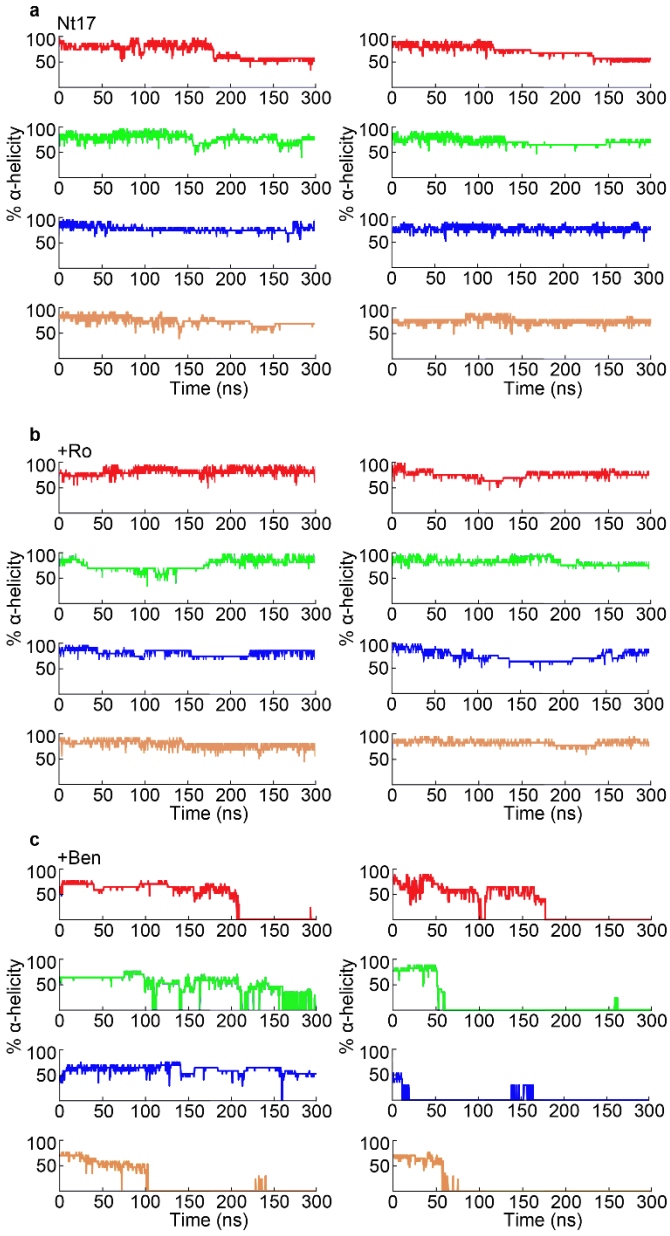

Figure 2.7 Percent α-helicity of each peptide in the **a**, Nt17 tetramer and **b**, Nt17 tetramer +Ro or **c**, +Ben for two additional simulations

When simulated in the absence of small molecules, the Nt17 tetramer was stable but displayed structural flexibility, as the helical content of each peptide would fluctuate to as low as ~50% helicity (Figure 2.5g and Figure 2.7a). Addition of ten Ro molecules stabilized the tetra-helical bundle by forming H-bonds with the compound (Figure 2.5h-j and Figure 2.7b). Residues sequestered within the tetramer structure did not readily form H-bonds with Ro. However, Ro had a strong preference for the C-terminal end of Nt17 peptides in the oligomer, and in particular H-bonded to S13 (~35% of the simulation time, Figure 2.5k and Figure 2.8). The H-bonds with S13 would typically form with the NH group of the first benzimidazole (labeled A in Figure 2.5h). To a lesser extent (~10% of the time), this NH group formed H-bonds with E12. Once Ro was positioned at S13 via H-bonding, the NH group of the second benzimidazole (labeled B in Figure 2.5h) and the 5-amine group of benzimidazole

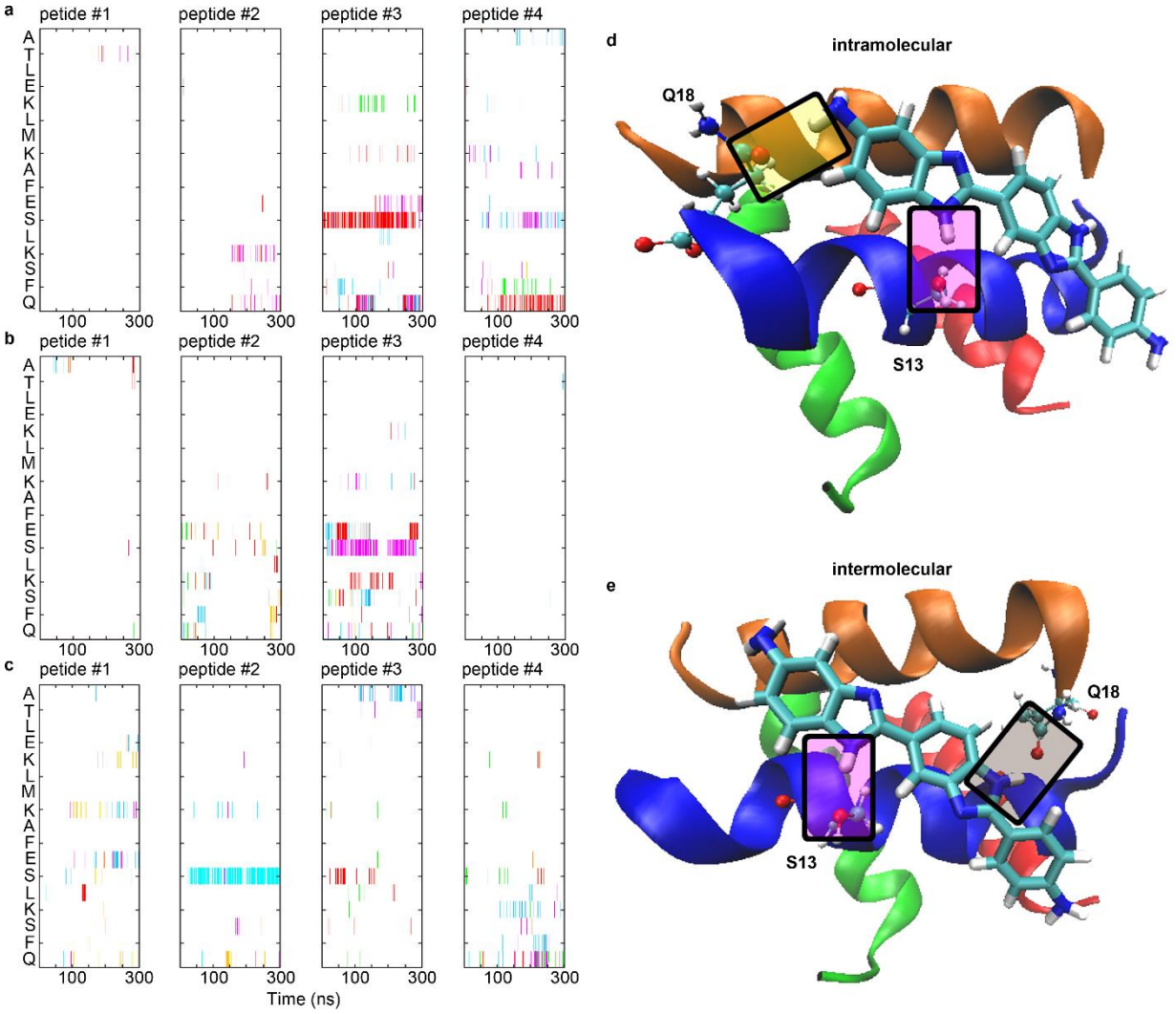

Figure 2.8 Hydrogen bonding profile of individual peptides within the Nt17 tetramer with Ro molecules. Each color represents an individual Ro molecule. **a,b** and **c** are three independent simulations. **d**, An example of an individual Ro molecule forming hydrogen bonds with S13 and Q18 within a single peptide (intramolecular). **e**, An example of an individual Ro molecule forming hydrogen bonds with S13 and Q18 from different peptides (intermolecular). For both examples, shaded boxes indicate the hydrogen bonds.

intermittently H-bonded with other residues (both intermolecularly and intramolecularly, (Figure 2.8d-e) with a preference for C-terminal residues and particularly Q18 (~15% of the simulation time). Similar to the interaction of Ro with monomers, additional Ro molecules would π-stack upon the Ro bound to Nt17 (Figure 2.5i). Overall, interaction

with Ro stabilized the α-helical structure of the C-terminal end of Nt17 peptides within the tetramer relative to the control (Figure 2.5l). The α-helix of Nt17 peptides in control simulations readily unfolded from the C-terminal end to E12, and the addition of Ro-90-7501, by associating with S13 and other C-terminal residues, significantly restricted this unfolding. This suggests structural flexibility at the C-terminal side of Nt17 plays a key role in htt oligomers binding membranes, consistent with recent cross-linking studies[19].

As S13 represented the primary site of association between htt and Ro, additional PDA/TBLE lipid binding assays were performed with a htt-exon1(46Q) construct containing a S13D mutation (Figure 2.9). Adding a negative charge at position 13 should strengthen the association between oligomers and Ro, enhancing the effectiveness of the compound to block htt/lipid interactions. Indeed, Ro reduced the CR associated with exposure to S13D htt-exon1(46Q) below 20% of control with doses as low as 0.1x (an ineffective dose with wild type htt). This was specific to Ro, as the S13D mutation had no impact on the efficiency of Ben to block htt binding to vesicles.

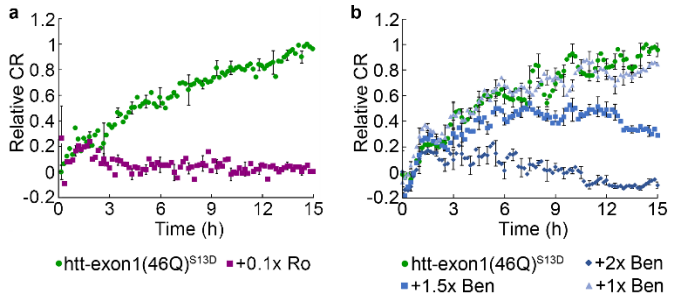

Figure 2.9 TBLE/PDA assay of htt-exon1(46Q)^{S13D}. **a**, TBLE/PDA vesicles exposed to htt-exon1(46Q)^{S13D} and 0.1x Ro. **b**, TBLE/PDA vesicles exposed to htt-exon1(46Q)^{S13D} and various doses of Benzamil. All signals are normalized with respect to TBLE/PDA vesicle exposure to 10 μM htt-exon1(46Q)^{S13D} and error bars represent SEM.

Ben interacted with Nt17 in a manner distinct from Ro (Figure 2.10a-d). In simulations with monomers, Nt17 completely unfolded within ~60-150 ns in five out of six simulations in the presence of three Ben molecules. While intermittent H-bonds formed between Ben and each residue within Nt17 (less than6% of simulation

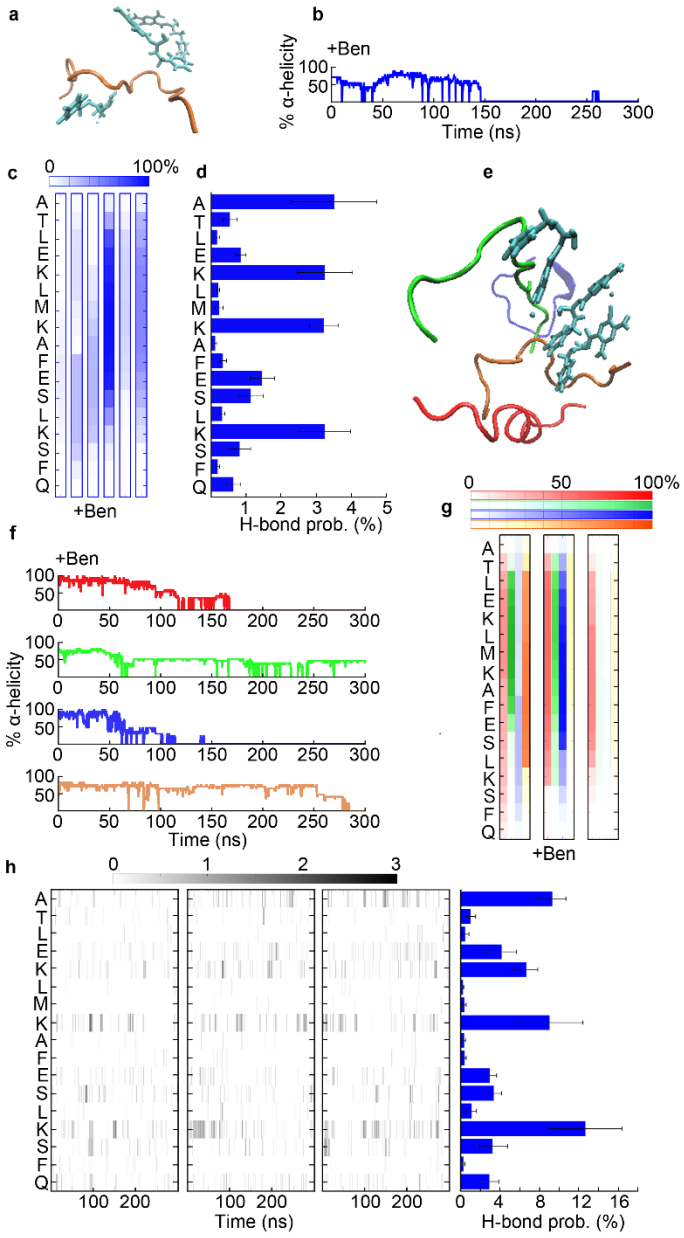

Figure 2.10 MD simulations of the interaction of Ben with Nt17. a, Nt17 monomer structure exposed to Ben after 150 ns of simulation. Nt17 is represented in orange and Ben in cyan. **b,** The percent α-helicity of Nt17 monomer in the presence of Ben as a function of time (five additional simulations provided in Figure 5). **c,** The average percent α-helicity of each residue in Nt17 monomers in the presence of Ben. For each condition, the individual heat maps represent an independent simulation. **d,** Residue specific hydrogen bonding probability density of Ben with Nt17 monomer averaged over six independent simulations., time-dependent hydrogen bonding profile and probability density of Ben with an Nt17 monomer for three independent simulations. **e,** Nt17 tetramer structure exposed to Ben molecules after 150 ns of simulation. **f,** The percent α-helicity of each Nt17 peptide within the tetramer structure upon exposure to Ben as a function of time (two additional simulations provided in Figure 6). **g,** The average percent α-helicity of each residue in Nt17 broken down by peptide within the tetramer structure in the presence of Ben. Three independent simulations are shown for each condition. Each column consists of 4 heat-maps representing the different Nt17 peptides (color coded). **h,** Residue specific, time-dependent hydrogen bonding profile and probability density of Ben with the Nt17 tetramer for three independent simulations. The color bar represents the number of H-bonds formed. All error bars represent SEM.

time for all residues), a slight preference for interacting with lysine residues (K6, K9, K15) and A2 due to the presence of the N-terminal amine group (Figure 2.10d). The lifetime of H-bonds with these amine-containing residues was typically longer on average (~0.5 nm

compared to ~0.3 ns for other residues). Overall, Ben appeared to have a minimal impact on the behavior of Nt17 monomers compared with control.

With Nt17 tetramers, the addition of Ben greatly destabilized the α-helical bundle structure (Figure 2.10e-g and Figure 2.7c); at least two or more α-helices were completely unfolded in each simulation. Nt17 peptides that were not completely unfolded by Ben displayed considerably less helicity compared with the control (Figure 2.10g). This unfolding allowed Ben to form intermittent H-bonds with all residues, and the preference for the N-terminal amine group and the three lysine residues remained (Figure 2.10h). However, H-bond formation with K15 was enhanced. K6 and K15 participate in salt bridges that stabilize htt oligomers[39], and Ben appears to interfere with these stabilizing interactions. Interestingly, this reduced stability of the tetramer structures with minimal impact on Nt17 monomers is consistent with the smaller oligomers observed via AFM (control oligomer mode height of 4-5 nm compared with oligomer mode height of 1.5-2.5 nm in the presence of Ben). As the development of helical structure in Nt17 is associated with lipid binding, the ability of Ben to destabilize the Nt17 α-helix would reduce the ability of htt to bind membranes.

2.3.4 Ro and Ben rescue phenotype in a C. elegans model of HD

To determine if Ro and Ben could ameliorate HD phenotype, both compounds were tested on a *C. elegans* model of HD, which express htt513 (slightly longer than exon1)[30]. The control strain, EAK102, expresses a polyQ stretch of 15 and will be referred to as Q15; EAK103 has a repeat glutamine stretch of 128 and will be referred to as Q128. Importantly, both are labeled with YFP at the C-terminal end of htt513, limiting the interference of this tag with the ability of Nt17 to bind lipids. Dosing of both compounds

was optimized by performing viability assays on WT *C. elegans* to determine the largest, nontoxic dose. Worms were treated with 150 µM of Ro and 150 µM of Ben. In age synchronized populations, the Q128 strain is less viable compared with Q15 as a function of time. Both Ro and Ben significantly ($p < 0.05$) increased viability of Q128 worms to Q15 levels by day 23 (Figure 2.11a). Beyond viability, Q128 worms develop a thrashing deficit as early as day 2 of adulthood. Treatment with Ro or Ben significantly improved ($p<0.01$) thrashing deficit on day 2 of adulthood and restored thrashing rates to control Q15 worm levels by day 7 (Figure 2.11b). Q128 worms develop visible inclusions of htt by day 2 of adulthood that do not form in Q15 worms. Despite improving viability and rescuing thrashing deficits, neither Ro or Ben prevented the development of these inclusions (Figure 2.11c-d), which is consistent with neither compound impacting fibril formation *in vitro.*

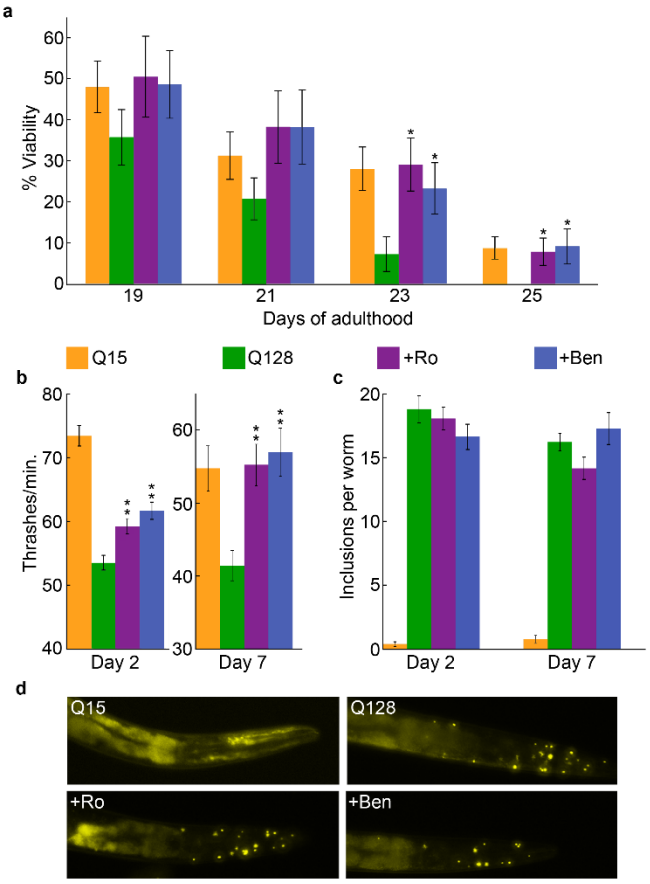

Figure 2.11 *C.elegans* model of HD a, Viability of Q15 and Q128 worms. Q128 worms were treated with either Ro or Ben. **b,** Thrashing rate measured in liquid media of Q128 worms untreated or treated with either Ro or Ben. Q15 worms were used as a control in all experiments. **c,** Number of inclusions formed per worm based on fluorescent microscopic images. **d,** Representative fluorescent images of Q15 worms and Q128 worms either untreated or treated with Ro or Ben. All error bars represent SEM and * indicates P<0.05 and ** indicates P<0.01

2.4 Discussion

Historically, modifying aggregation has been a popular strategy for developing therapeutics for amyloid-based diseases. While numerous methods to alter aggregation have been developed, ranging from small molecules to antibodies[40–43], this strategy has not yielded an effective therapeutic. Of interest here, many small molecule aggregation inhibitors lose their effectiveness in the presence of membranes[16,44]. Strikingly, many amyloid proteins readily associate with and damage a variety of cellular membranes. Here, a novel strategy was developed that targets the ability of amyloid-forming proteins from directly interacting with lipid membranes. Using htt-exon1 as a model system, two compounds were identified, their mechanism of action explored, and their ability to rescue phenotype in a *C. elegans* model of HD demonstrated. Collectively, this study serves as a proof of principle for this approach.

Ro has been identified as a potentially generic inhibitor of amyloid formation. In this regard, Ro effectively inhibits both Aβ and α-syn aggregation[35,36]. While ThT data suggests that Ro competitively bound to fibrils, it was not effective in modifying htt aggregation. As htt fibrils exhibit limited ability to bind lipid vesicles and the screens were performed with non-fibrillar htt, the ability to bind fibrils does not appear to be the major factor in blocking htt/lipid interactions. MD simulations suggested that Ro has a high propensity to localize to S13 in Nt17 in both monomeric and oligomeric forms of htt. Additional molecules of Ro can subsequently π-stack on top of the Nt17 bound Ro. This π-stacking may provide shielding between polar residues that facilitate the initial steps in htt monomers binding to membranes[45]. Within oligomers, the Ro molecule bound to S13 forms intermittent hydrogen bonds (both intra- and intermolecular) with other residues

toward the C-terminus of Nt17. These contacts stabilize the α-helical structure of Nt17 and reduce the configurational flexibility of the oligomer. Cross-linking studies suggest that configurational flexibility plays an important role in the ability of htt oligomers to bind lipid membranes[19]. The importance of the ability of Ro-90-7501 to localize to S13 is experimentally supported by the enhanced efficacy of blocking htt/lipid interaction of htt containing a S13D mutation.

Ben has been shown to reduce htt-induced toxicity in cellular models and mouse models[46]. Ben, as an acid sensing ion channel blocker, reduced htt toxicity in HD mice by reducing acidosis and enhancing ubiquitin proteosome activity. Our study suggests that Ben also directly interacts with htt, blocking its ability to bind membranes and providing additional protection. The mechanism by which Ben blocks htt from binding membranes differs from that of Ro. Based on MD simulations, Ben uncoils the α-helical oligomer structure by preferentially interacting with amine groups at the N-terminus and in lysine residues of Nt17. Lysine residues in Nt17 are highly protected in aggregate structures[39], suggesting they are involved in stabilizing interactions such as salt bridges. However, the interaction of Ben with monomers is much weaker compared with oligomers. Collectively, this results in slightly smaller oligomers as the rate of dissociation is slightly increased while the association rate is mostly unaffected. However, a steady population of oligomers develops, resulting in no impact of fibril formation. The destabilization of the underlying α-helical structure may underscore the reduced affinity for lipid membranes. It is also possible that by localizing near Lysine residues that Ben blocks electrostatic interactions between Lysine and anionic headgroups of lipids. This is consistent with acetylation of these lysine residues reducing the affinity of htt for lipids[47]. The apparent disparate modes

of action by which Ro and Ben block htt/lipid interactions points to a multi-faceted mechanism by which htt monomers and oligomers bind and disrupt membranes.

Despite improving phenotype in *C. elegans*, neither drug eliminated inclusion formation. As neither drug had an inhibitory impact on fibril formation *in vitro*, this is not surprising. However, the situation *in vivo* is likely more complicated. Lipid membranes have a varied impact on htt aggregation depending on lipid composition. POPC, POPS, DMPC, POPG, and POPC/POPS mixed systems all promote fibril formation[14,17,18]. DOPC, POPE, TBLE, cardiolipin, inner and outer mitochondrial mimics, and other cellular extracts decrease fibril formation[17,18,48,49]. With TBLE and other cellular extracts decreasing aggregation, htt association with lipid membranes *in vivo* may slow aggregation into inclusions. As such, blocking htt from those membranes may enhance inclusion formation. This notion that impeding the ability of htt to bind membranes would enhance aggregation is supported by the observation that removing Nt17 from htt-exon1 expressed in cells enhances inclusion formation and the efficiency of seeding aggregation with pre-formed aggregates[50]. Additionally, crowded aqueous environments (similar to the cytosol) at membrane/liquid interfaces further modifies htt aggregation on membranes in a manner dependent on crowding agents[51].

This approach of blocking the ability of amyloid-forming proteins to directly interact with lipid membranes can be extended toward other amyloid-based disease and biological processes. Lipids are a common modulator of amyloid formation, as studies of α-synuclein[52], islet amyloid polypeptide, β-amyloid[53], and polyQ[12,14,54] all demonstrate altered aggregation in the presence of membranes and the ability to induce physical damage to membranes. This notion is supported by recent reports that the natural

products, squalamine and trodusquemine, ameliorate α-synuclein and Aβ toxicity associated with PD and AD respectively by displacing oligomers from membranes[55,56]. With regard to Aβ, squalamine and its derivatives ameliorated Aβ-induced toxicity despite increasing amyloid formation[57]. The mechanism of action of these natural products is via changing membrane properties[56]. Our strategy targets protein aggregates directly, gaining specificity. Additionally, amyloids function in viral and bacterial infection, potentially via membrane interaction. For example, amyloid aggregates of PAP248-286 in human semen severely increase infection efficiency of HIV[58] as PAP248-286 fibrils promote interaction between the lipid membrane of the HIV virion with the host membrane[59]. Murine cytomegalovirus protein M45[60], NSs (Rift Valley fever virus)[61], and the gut bacterial protein curli[62] are functional amyloids associated with infection. Thus, targeting the ability of amyloids to bind and damage membranes may find broad utility as a therapeutic strategy.

2.5 References

1. Harrison, R. S., Sharpe, P. C., Singh, Y. & Fairlie, D. P. Amyloid peptides and proteins in review. in *Reviews of Physiology, Biochemistry and Pharmacology* (eds. Amara, S. G. et al.) 1–77 (Springer Berlin Heidelberg, 2007). doi:10.1007/112_2007_0701.
2. Zaman, M., Khan, A. N., Wahiduzzaman, Zakariya, S. M. & Khan, R. H. Protein misfolding, aggregation and mechanism of amyloid cytotoxicity: An overview and therapeutic strategies to inhibit aggregation. *International Journal of Biological Macromolecules* **134**, 1022–1037 (2019).
3. Burke, K. A., Yates, E. A. & Legleiter, J. Biophysical Insights into How Surfaces, Including Lipid Membranes, Modulate Protein Aggregation Related to Neurodegeneration. *Front. Neurol.* **4**, (2013).
4. Yasumoto, T. *et al.* High molecular weight amyloid β $_{1\text{-}42}$ oligomers induce neurotoxicity *via* plasma membrane damage. *FASEB j.* **33**, 9220–9234 (2019).
5. Ericsson, M. *et al.* Crowded organelles, lipid accumulation, and abnormal membrane tubulation in cellular models of enhanced α-synuclein membrane interaction. *Brain Research* **1758**, 147349 (2021).

6. Chua, C. E. L. & Tang, B. L. Rabs, SNAREs and α-synuclein — Membrane trafficking defects in synucleinopathies. *Brain Research Reviews* **67**, 268–281 (2011).
7. Liu, K.-Y. *et al.* Disruption of the nuclear membrane by perinuclear inclusions of mutant huntingtin causes cell-cycle re-entry and striatal cell death in mouse and cell models of Huntington's disease. *Human Molecular Genetics* **24**, 1602–1616 (2015).
8. Gasset-Rosa, F. *et al.* Polyglutamine-Expanded Huntingtin Exacerbates Age-Related Disruption of Nuclear Integrity and Nucleocytoplasmic Transport. *Neuron* **94**, 48-57.e4 (2017).
9. Bäuerlein, F. J. B. *et al.* In Situ Architecture and Cellular Interactions of PolyQ Inclusions. *Cell* **171**, 179-187.e10 (2017).
10. Riguet, N. *et al.* Nuclear and cytoplasmic huntingtin inclusions exhibit distinct biochemical composition, interactome and ultrastructural properties. *Nat Commun* **12**, 6579 (2021).
11. Yan, S. *et al.* A Huntingtin Knockin Pig Model Recapitulates Features of Selective Neurodegeneration in Huntington's Disease. *Cell* **173**, 989-1002.e13 (2018).
12. Burke, K. A., Kauffman, K. J., Umbaugh, C. S., Frey, S. L. & Legleiter, J. The Interaction of Polyglutamine Peptides with Lipid Membranes Is Regulated by Flanking Sequences Associated with Huntingtin. *Journal of Biological Chemistry* **288**, 14993–15005 (2013).
13. Michalek, M., Salnikov, E. S. & Bechinger, B. Structure and Topology of the Huntingtin 1–17 Membrane Anchor by a Combined Solution and Solid-State NMR Approach. *Biophysical Journal* **105**, 699–710 (2013).
14. Pandey, N. K. *et al.* The 17-residue-long N terminus in huntingtin controls stepwise aggregation in solution and on membranes via different mechanisms. *Journal of Biological Chemistry* **293**, 2597–2605 (2018).
15. Jayaraman, M. *et al.* Slow Amyloid Nucleation via α-Helix-Rich Oligomeric Intermediates in Short Polyglutamine-Containing Huntingtin Fragments. *Journal of Molecular Biology* **415**, 881–899 (2012).
16. Beasley, M. *et al.* Lipid Membranes Influence the Ability of Small Molecules To Inhibit Huntingtin Fibrillization. *Biochemistry* **58**, 4361–4373 (2019).
17. Beasley, M., Groover, S., Valentine, S. J. & Legleiter, J. Lipid headgroups alter huntingtin aggregation on membranes. *Biochimica et Biophysica Acta (BBA) - Biomembranes* **1863**, 183497 (2021).
18. Beasley, M. *et al.* Physicochemical Properties Altered by the Tail Group of Lipid Membranes Influence Huntingtin Aggregation and Lipid Binding. *J. Phys. Chem. B* **126**, 3067–3081 (2022).
19. Sedighi, F. *et al. Oligomerization enhances huntingtin membrane activity but is suppressed by covalent crosslinking*. http://biorxiv.org/lookup/doi/10.1101/2023.03.01.530665 (2023) doi:10.1101/2023.03.01.530665.
20. Thompson, L. M. *et al.* IKK phosphorylates Huntingtin and targets it for degradation by the proteasome and lysosome. *Journal of Cell Biology* **187**, 1083–1099 (2009).
21. Zheng, F., Wu, Z. & Chen, Y. A quantitative method for the measurement of membrane affinity by polydiacetylene-based colorimetric assay. *Analytical Biochemistry* **420**, 171–176 (2012).

22. Dutta, S., Watson, B., Mattoo, S. & Rochet, J.-C. Calcein Release Assay to Measure Membrane Permeabilization by Recombinant Alpha-Synuclein. *BIO-PROTOCOL* **10**, (2020).
23. Burke, K. A., Godbey, J. & Legleiter, J. Assessing mutant huntingtin fragment and polyglutamine aggregation by atomic force microscopy. *Methods* **53**, 275–284 (2011).
24. Kotler, S. A. *et al.* Probing initial transient oligomerization events facilitating Huntingtin fibril nucleation at atomic resolution by relaxation-based NMR. *Proc Natl Acad Sci USA* **116**, 3562–3571 (2019).
25. Jo, S., Kim, T., Iyer, V. G. & Im, W. CHARMM-GUI: A web-based graphical user interface for CHARMM. *J. Comput. Chem.* **29**, 1859–1865 (2008).
26. Martínez, L., Andrade, R., Birgin, E. G. & Martínez, J. M. PACKMOL: A package for building initial configurations for molecular dynamics simulations. *J. Comput. Chem.* **30**, 2157–2164 (2009).
27. Humphrey, W., Dalke, A. & Schulten, K. VMD: Visual molecular dynamics. *Journal of Molecular Graphics* **14**, 33–38 (1996).
28. Vanommeslaeghe, K. *et al.* CHARMM general force field: A force field for drug-like molecules compatible with the CHARMM all-atom additive biological force fields. *J. Comput. Chem.* NA-NA (2009) doi:10.1002/jcc.21367.
29. Phillips, J. C. *et al.* Scalable molecular dynamics with NAMD. *J. Comput. Chem.* **26**, 1781–1802 (2005).
30. Lee, A. L., Ung, H. M., Sands, L. P. & Kikis, E. A. A new Caenorhabditis elegans model of human huntingtin 513 aggregation and toxicity in body wall muscles. *PloS one* **12**, e0173644 (2017).
31. Corsi, A. K. A Transparent window into biology: A primer on Caenorhabditis elegans. *WormBook* 1–31 (2015) doi:10.1895/wormbook.1.177.1.
32. Mitchell, D. H., Stiles, J. W., Santelli, J. & Sanadi, D. R. Synchronous growth and aging of Caenorhabditis elegans in the presence of fluorodeoxyuridine. *Journal of gerontology* **34**, 28–36 (1979).
33. Schindelin, J. *et al.* Fiji: an open-source platform for biological-image analysis. *Nat Methods* **9**, 676–682 (2012).
34. Nussbaum-Krammer, C. I., Neto, M. F., Brielmann, R. M., Pedersen, J. S. & Morimoto, R. I. Investigating the Spreading and Toxicity of Prion-like Proteins Using the Metazoan Model Organism C. elegans. *JoVE* 52321 (2015) doi:10.3791/52321.
35. Bohrmann, B. *et al.* Self-Assembly of β-Amyloid 42 Is Retarded by Small Molecular Ligands at the Stage of Structural Intermediates. *Journal of Structural Biology* **130**, 232–246 (2000).
36. Braun, A. R. *et al.* Potent inhibitors of toxic alpha-synuclein identified via cellular time-resolved FRET biosensors. *npj Parkinsons Dis.* **7**, 52 (2021).
37. Chalfant, M. L., Peterson-Yantorno, K., O'Brien, T. G. & Civan, M. M. Regulation of epithelial Na+ channels from M-1 cortical collecting duct cells. *American Journal of Physiology-Renal Physiology* **271**, F861–F870 (1996).
38. Gomez-Sanchez, E. P. & Gomez-Sanchez, C. E. Effect of central infusion of benzamil on Dahl S rat hypertension. *American Journal of Physiology-Heart and Circulatory Physiology* **269**, H1044–H1047 (1995).

39. Arndt, J. R., Brown, R. J., Burke, K. A., Legleiter, J. & Valentine, S. J. Lysine residues in the N-terminal huntingtin amphipathic α-helix play a key role in peptide aggregation. *Journal of Mass Spectrometry* **50**, 117–126 (2015).
40. Ehrnhoefer, D. E. *et al.* EGCG redirects amyloidogenic polypeptides into unstructured, off-pathway oligomers. *Nat Struct Mol Biol* **15**, 558–566 (2008).
41. Heiser, V. *et al.* Inhibition of huntingtin fibrillogenesis by specific antibodies and small molecules: Implications for Huntington's disease therapy. *Proc. Natl. Acad. Sci. U.S.A.* **97**, 6739–6744 (2000).
42. Legleiter, J. *et al.* Effect of Different Anti-Aβ Antibodies on Aβ Fibrillogenesis as Assessed by Atomic Force Microscopy. *Journal of Molecular Biology* **335**, 997–1006 (2004).
43. Yang, F. *et al.* Curcumin Inhibits Formation of Amyloid β Oligomers and Fibrils, Binds Plaques, and Reduces Amyloid in Vivo. *Journal of Biological Chemistry* **280**, 5892–5901 (2005).
44. Engel, M. F. M. *et al.* The Polyphenol EGCG Inhibits Amyloid Formation Less Efficiently at Phospholipid Interfaces than in Bulk Solution. *J. Am. Chem. Soc.* **134**, 14781–14788 (2012).
45. Côté, S., Wei, G. & Mousseau, N. Atomistic mechanisms of huntingtin N-terminal fragment insertion on a phospholipid bilayer revealed by molecular dynamics simulations: htt $^{NT}Q_{N}$ Insertion on a Phospholipid Bilayer. *Proteins* **82**, 1409–1427 (2014).
46. Wong, H. K. *et al.* Blocking acid-sensing ion channel 1 alleviates Huntington's disease pathology via an ubiquitin-proteasome system-dependent mechanism. *Human Molecular Genetics* **17**, 3223–3235 (2008).
47. Chaibva, M. *et al.* Acetylation within the first 17 residues of huntingtin exon 1 alters aggregation and lipid binding. *Biophysical journal* **111**, 349–362 (2016).
48. Adegbuyiro, A. *et al.* Mitochondrial membranes modify mutant huntingtin aggregation. *Biochimica et Biophysica Acta (BBA) - Biomembranes* **1863**, 183663 (2021).
49. Levy, G. R. *et al.* Huntingtin's N-Terminus Rearrangements in the Presence of Membranes: A Joint Spectroscopic and Computational Perspective. *ACS Chem. Neurosci.* **10**, 472–481 (2019).
50. Lee, C. Y. D. *et al.* Disease-related Huntingtin seeding activities in cerebrospinal fluids of Huntington's disease patients. *Sci Rep* **10**, 20295 (2020).
51. Groover, S. E. *et al.* Macromolecular crowding in solution alters huntingtin interaction and aggregation at interfaces. *Colloids and Surfaces B: Biointerfaces* **206**, 111969 (2021).
52. Ruipérez, V., Darios, F. & Davletov, B. Alpha-synuclein, lipids and Parkinson's disease. *Progress in Lipid Research* **49**, 420–428 (2010).
53. Knight, J. D. & Miranker, A. D. Phospholipid Catalysis of Diabetic Amyloid Assembly. *Journal of Molecular Biology* **341**, 1175–1187 (2004).
54. Burke, K. A., Yates, E. A. & Legleiter, J. Amyloid-Forming Proteins Alter the Local Mechanical Properties of Lipid Membranes. *Biochemistry* **52**, 808–817 (2013).
55. Limbocker, R. *et al.* Squalamine and trodusquemine: two natural products for neurodegenerative diseases, from physical chemistry to the clinic. *Nat. Prod. Rep.* **39**, 742–753 (2022).

56. Perni, M. *et al.* A natural product inhibits the initiation of α-synuclein aggregation and suppresses its toxicity. *Proc. Natl. Acad. Sci. U.S.A.* **114**, (2017).
57. Limbocker, R. *et al.* Squalamine and Its Derivatives Modulate the Aggregation of Amyloid-β and α-Synuclein and Suppress the Toxicity of Their Oligomers. *Front. Neurosci.* **15**, 680026 (2021).
58. Usmani, S. M. *et al.* Direct visualization of HIV-enhancing endogenous amyloid fibrils in human semen. *Nat Commun* **5**, 3508 (2014).
59. Brender, J. R. *et al.* Helical Conformation of the SEVI Precursor Peptide PAP248-286, a Dramatic Enhancer of HIV Infectivity, Promotes Lipid Aggregation and Fusion. *Biophysical Journal* **97**, 2474–2483 (2009).
60. Pham, C. L. *et al.* Viral M45 and necroptosis-associated proteins form heteromeric amyloid assemblies. *EMBO Reports* **20**, (2019).
61. Léger, P. *et al.* NSs amyloid formation is associated with the virulence of Rift Valley fever virus in mice. *Nat Commun* **11**, 3281 (2020).
62. Sampson, T. R. *et al.* A gut bacterial amyloid promotes α-synuclein aggregation and motor impairment in mice. *eLife* **9**, e53111 (2020).

Chapter 3 Ruthenium red impedes huntingtin aggregation and blocks its interaction with membranes with potential therapeutic benefit.

3.1 Introduction

Amyloid formation leading to proteinaceous deposits within tissues is a major hallmark of many neurodegenerative diseases like Alzheimer's disease (AD), Parkinson's disease (PD), and Huntington's disease (HD)[1,2]. Amyloids form via a nucleation dependent process and exhibit rigid fibrillar structures having a cross β- morphology that can withstand chemical and thermal degradation[3–5]. During aggregation a mixture of intermediate aggregates species are formed such as small oligomers and protofibrils[2,6,7]. Since distinct aggregates are implicated to varying degrees in cellular toxicity, a common strategy to develop therapeutics is inhibiting or modulating the process of aggregation[8]. However, this approach has had limited success. Most amyloid forming proteins directly interact with lipid membranes, which can alter the aggregation process and result in membrane damage. For instance, Aβ oligomers and protofibrils interact with cell membranes via distinct mechanisms that have been linked to neuronal toxicity[9]. Oligomers of α-synuclein bind membranes with high affinity and cause membranal damage[10]. As aggregates associated with amyloid formation damage membranes, blocking these interactions represents a potential therapeutic strategy.

HD is a genetic neurodegenerative disease caused by the abnormal expansion of a polyglutamine (polyQ) tract near the N -terminus of the huntingtin (htt) protein[11]. PolyQ expansion beyond a critical threshold (~35 repeats) results in HD, and repeat length correlates with age of onset and disease severity[12]. Expanded polyQ induces htt

aggregation into fibrils and a variety of different aggregate types including oligomers, annular aggregates, and amorphous aggregates with varying degrees of toxicity[2]. Htt aggregation is a complex process, and the relative importance of toxic mechanisms associated with specific aggregates is not yet fully understood.

As commonly observed with other amyloid proteins, htt strongly interacts with various membranous surfaces. These interactions alter membranes in a manner consistent with a variety of toxic mechanisms. For example, a knock in mouse model of HD suggest htt directly binds the outer mitochondrial membrane leading to an alteration in calcium retention capacity[13]. This is further illustrated by electron micrographs of mutant htt interacting with neuronal mitochondrial membranes and causing calcium handling defects[14]. In addition, htt fibrils and inclusions imping on the endoplasmic reticulum (ER), causing deformations in the membrane and altered ER dynamics[15,16]. Furthermore, perinuclear inclusions of htt disrupt the nuclear envelope resulting in striatal cell death in HD mouse models[17]. Mutant htt disrupt and mechanically damage model lipid bilayers, as demonstrated by *in situ* AFM and membrane leakage assays[18–22]. For these *in vitro* studies, membrane composition modifies these interactions also plays an important. Total brain lipid extract (TBLE) bilayers reduce fibril formation and promote oligomer stability [21,22]. Enriching TBLE bilayers with alters aggregation directly on the bilayer and considerably reduces htt induced membrane damage[21]. Increasing either sphingomyelin (SM) or ganglioside (GM1) content in TBLE decreases htt membrane insertion, yet increased SM content enhanced htt- membrane permeabilization while GM1 had no impact[21,22].

In htt, the polyQ domain is flanked on its N-terminal side by the first 17 amino acids of exon1 (Nt17) and a proline rich domain on its C-terminus end[23]. Both of these domains alter aggregation in bulk solution. Nt17 enhances fibril formation by promoting α-helix rich oligomers[24,25]. The proline rich domain slows fibril formation by stabilizing the polyQ domain[26]. Beyond its impact on aggregation, Nt17 serves as a lipid binding domain[27–29]. Nt17 is intrinsically disordered in bulk solution but folds into an amphipathic α-helix when binding membranes[28,29]. Molecular dynamic simulations reveal that first contacts with the phospholipid head groups are established via the hydrophilic residues of Nt17 α-helix[28,30,31]. Then a reorganizing step resulting an structural change to bring non polar residues near the membrane core followed by an anchoring step occurs where nonpolar residues such as phenylalanine move towards the core of the lipid membrane[30,31]. Finally other non-polar residues are partitioned into the membrane.[30,31]

During the screen described in Chapter 2, an additional molecule (ruthenium red) that inhibited the interaction of htt-exon1 with lipid membranes was identified. Due to its unique structure and chemical properties compared to Ro 90-7501 and Benzamil hydrochloride, it was further investigated separately. Ruthenium red (ammoniated ruthenium oxychloride) is an inorganic complex. Unlike Ro 90-7501 and Benzamil hydrochloride, ruthenium red promiscuously binds numerous proteins, especially Ca^{2+} binding proteins[32–34]. Importantly, ruthenium complexes are generally non-toxic[35–37] and readily interact with a several amyloids[38–44]. Complexes containing ruthenium inhibit the aggregation of human islet amyloid polypeptide (hIAPP) and break down fibrils of hIAPP[40]. Ruthenium complexes also disaggregate prion neuropeptide PrP106–126[39]. Here, a detailed analysis of the impact of ruthenium red on htt-exon1 aggregation and

membrane binding was conducted. In addition, the ability of ruthenium red to alter HD phenotype in a *C. elegans* model was determined.

3.2 Methods

3.2.1 Purification of GST-htt-exon1 fusion protein

Glutathione *S*-transferase (GST)-htt-exon1 fusion protein with 46 glutamine repeat units was purified as described previously[45]. In brief, GST-htt exon 1 (htt) was expressed in *Escherichia coli* by induction with isopropyl *β*-D- thiogalactoside at 30 °C for 4 h. Cells were lysed with a combination of lysozymes (0.5mg/mL) and probe sonication. The protein was purified from the lysate with a GST affinity column using LPLC, Bio-rad liquid chromatography. Relevant fractions were identified using ultraviolet absorption and confirmed by gel electrophoresis. The protein was subjected to dialysis for 48 h. Before use in any assay, the protein was centrifuged for 30 min at 20000 ×g at 4 °C to remove preexisting fibrils. Factor Xa (New England Biolabs) was used to cleave the GST tag. All experiments were carried out in a buffer composed of 50 mM Tris-HCl, 150 mM NaCl.

3.2.2 TBLE/PDA assay

TBLE/PDA assays were performed as reported previously[46]. Shortly, TBLE (Avanti lipids) and 10,12 tricosadiynoic acid were combined in a molar ratio of 2:3 in an ethanol/chloroform mixture. Solutions were dried under a stream of N_2 for 15 min. The resulting film was re-suspended in 50 mM tris buffered saline at 70 °C. After 5 min of probe sonication, solutions were stored at 4 °C overnight to allow self-assembly of vesicles. The diacetylene monomers were polymerized by irradiation under 254 nm for 15 min. Prior to use in TBLE/PDA assay, htt-exon1(46Q) was incubated on ice with Factor

Xa for 90 minutes to allow cleavage and formation of oligomers. Final concentration of htt-exon1(46Q) in TBLE/PDA assays was 10 μM and ruthenium red added to obtain concentrations of 1x, 2x and 4x with respect to of htt-exon1(46Q). htt lipid interactions were measured fluorescently at room temperature with excitation and emission wavelengths of 485 and 560 nm respectively for 18 h at 10 min time intervals utilizing a SpectraMax M2 Multi-Mode plate reader. Experiments were carried out in 96-well plated at 25 ºC.

3.2.3 Thioflavin T (ThT) assay

ThT assays were conducted in 96- well plates on a Spectramax M2 microplate reader. Final ThT concentration in each well was 40 μg/mL. The aggregation of htt-exon1(46Q) in the presence of varying doses ruthenium red was investigated by measuring ThT fluorescence. For the investigation of aggregation in the presence of lipid vesicles in addition to htt-exon1(46Q) and ruthenium red, TBLE lipid vesicles were added to a final lipid concentration of 200 μM TBLE. (1:20 htt : lipid). ThT fluorescence was measured at 484 nm emission (440 nm excitation) at 37 °C for 18 h with readings taken every 10 min time intervals. All experimental conditions were performed in triplicates.

3.2.4 Filter trap assay

Htt-exon1(46Q)(10 μM) was incubated with 1x and 4x of ruthenium red with respect to htt concentration. Htt alone was used a control. Incubations were maintained at 37ºC. 6 μL aliquots were drawn from each incubation at 1 h, 3 h, 5 h and 8 h to 0.5% sodium dodecyl sulfate and boiled for 5 mins. Boiled samples were allowed to cool to room temperature and serially diluted to obtain 1.2, 0.6 ug and 0.3 ug of htt. Samples were deposited on to

a pre wet nitrocellulose membrane of 0.45 um pore size that was assembled on a slot blot manifold. After all loaded sample were pulled through the membrane by vacuum, the membrane was carefully removed, dried at room temperature, and soaked overnight in blocking buffer (5% milk solution in TBS) at 4 ^{o}C. Membrane was then incubated with htt-specific monoclonal primary antibody, MW8 (Developmental Studies Hybridoma Bank,1:350 dilution) on an orbital shaker for 1 h at room temperature. After washing the membranes with TBS the membranes were probed for 1 h with secondary goat anti-mouse alkaline phosphate antibody at 1:500 dilution. Color development was obtained using BCIP/NBT substrate incubating for 15 min.

3.2.5 Atomic force microscopy (AFM)

All AFM imaging was performed with a Nanoscope V Multimode atomic force microscope (Veeco, Santa Barbara, CA) equipped with a closed-loop vertical engage J-scanner. For AFM experiments to determine the impact of ruthenium red on aggregation, htt-exon1(46Q) (10µM) was incubated with ruthenium red (1x and 4x) at 37 $^{\circ}$C and sampled after 1 h, 3 h, 5 h and 8h for imaging. Htt-exon1(46Q)(10µM) was used as a control. At each time point, a 5 µL aliquot of each sample was deposited on freshly cleaved mica, allowed to set for 1 min, washed with ultrapure water, and dried with a stream of air. Imaging was done using silicon oxide cantilevers with a normal spring constant of ~40 N/m and resonance frequency of ~300 kHz at a scan rate of ~2Hz.

3.2.6 *C.elegans*

Two *C.elegans* strains EAK 102 expressing htt-513(Q15) and EAK 103 expressing htt-513(Q128)[47] were obtained from Caenorhabditis Genetics Center. Worms were

maintained at 20 °C in NGM plates inoculated with OP50 under standard techniques. Age synchronized worms were obtained using previously described methods[48]. EAK 102 (Q15) serves only as a control in all experiments while EAK 103 (Q128) was treated ruthenium red. For thrashing assays, ruthenium red (20 µM and 40 µM) induced NGM plates (35 mm diameter) were prepared with a final FUdR concentration of 400 µM. For each plate ~100 age synchronized L4 worms were introduced and were maintained at 20 °C. Thrashing rate was observed on day 2 and 7 of the adulthood. Animals were picked from plates in 25 µL drops of M9 buffer and placed on a microscopic slide. They were given 30 s recovery time, and a 1 min video of their thrashing in liquid was recorded. The videos were processed and analyzed using MATLAB image processing toolbox and Image J equipped with worm tracker plugin[49,50]. A minimum of 35 animals were assessed for each condition per trial.

To measure inclusion formation via fluorescent microscopy, adult day 7 animals were obtained from NGM plates and were suspended in 15 mg/ mL 2,3-Butanedione monoxime (BDM) for 30-60 mins to induce paralysis in worms. Once paralyzed the worms were imaged in solution with either 10x magnification or 20x magnification. Inclusion counts in each image was determined by counting the fluorescent foci in each worm.

3.3 Results

3.3.1 Ruthenium red inhibits htt/lipid binding in a dose dependent manner.

Ruthenium red, having been identified by the screen described in Chapter 2, was retested with a kinetic PDA/TBLE vesicle binding assay. In this assay, the ability of a 10x dose of ruthenium red to reduce the interact of 10 µM htt-exon1(46Q) with PDA/TBLE

vesicles by at least 80% was confirmed. Next, the dose dependency of ruthenium red to inhibit htt/lipid interactions was determined with additional PDA/TBLE assays (10 μM htt with a protein to lipid ratio of 1:20). Here, a fluorescence-based PDA assay was performed to control for the red color of ruthenium red instead of the absorbance-based assay. With 4x ruthenium red, the PDA fluorescence response was reduced by ~95% after 18 h with respect to the htt-exon1(46Q) control. With decreasing dose of ruthenium red, the ability to block htt-exon1(46Q) from binding lipids was reduced, as 2x and 1x doses resulted in reduction of PDA fluorescence to ~90% and 75% respectively. The reduced PDA signal was statistically ($p<0.01$) significant for each condition tested. While ruthenium red can bind highly anionic membranes[51], the PDA assay suggests that it does not readily bind TBLE, as it did not produce a PDA response. Instead, this suggests that ruthenium red is readily interacting with htt-exon1(46Q).

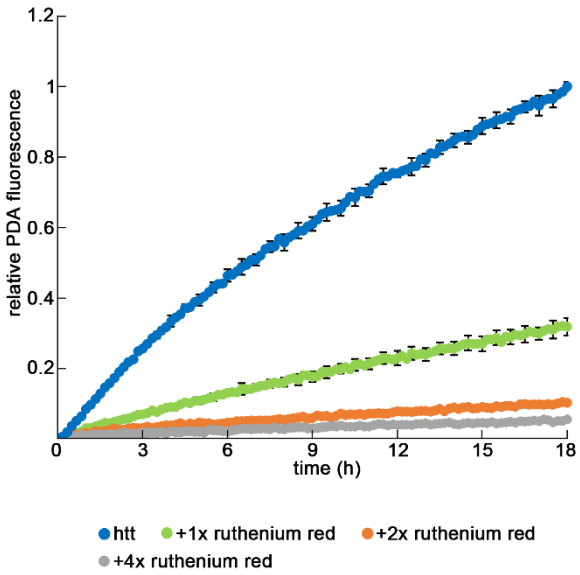

Figure 3.1 Impact of ruthenium red on htt lipid binding, Relative fluorescence of PDA/TBLE vesicles exposed to htt exon 1 (46Q) (10 μM) measured kinetically in the presence of varying doses of ruthenium red. Error bars represent SEM.

3.3.2 Ruthenium red alters htt aggregation in a dose dependent manner.

With ruthenium red being known to promiscuously bind proteins and the PDA assays suggesting that ruthenium red may be directly interacting with htt-exon1(46Q), a series of assays were performed to determine if it impacted htt-exon1(46Q) aggregation. Htt-exon1(46Q) (10 μM) was incubated at 37 °C with either 1x, 2x or 4x doses of ruthenium red. These doses were based on their ability to readily block htt/lipid interactions. Htt-exon1(46Q) aggregation in the absence of ruthenium red served as control. Fibril formation was monitored using a ThT assay which exhibits enhanced fluorescence efficiency upon binding the cross β-structure associated with amyloid. Based on the ThT assay, ruthenium red inhibited fibrilization in a dose dependent manner. 1x ruthenium red, htt fibrilization was significantly ($p < 0.01$) reduced by ~25%. Increasing the ruthenium red dose to 2x and 4x enhanced fibril inhibition by ~80% and ~90% respectively. (Figure 2a) As lipids are known to interfere with the ability of some small molecules to inhibit htt-exon1 aggregation[52], additional ThT assays were performed to determine if ruthenium red was an effective amyloid inhibitor in the presence of TBLE vesicles. For these assays, the htt to lipid ratio was 1:20. With the presence of TBLE ruthenium red still significantly inhibited htt fibrilization in a dose dependent manner. 1x ruthenium red resulted in a ~25% reduction in Tht signal, 2x reduced it by ~60 %, and 4x led to ~80 % decreased signal. (Figure 2b)

To further validate the ability of ruthenium red to inhibit fibril formation, a filter trap assay was performed. Htt-exon1(46Q) (10 μM) was incubated with the presence of 1x and 4x Ruthenium red, boiled in SDS and was passed through a nitrocellulose membrane

with a pore size of ~0.45 µm, trapping large, SDS-insolbule aggregates (fibrils) and allowing small species to pass. Htt-exon1(46Q) alone was used as a control. Incubations were sampled at 1 h, 3 h 5 h and 8 h and deposited on the membrane with serial dilutions (1.2 µg 0.6 µg and 0.3 µg). The membrane was probed with the MW8 anti-htt antibody which detects the C-terminal residues of htt-exon1[53]. This epitope presents on the periphery of fibrils and is readily available for recognition by MW8[54]. In the htt-exon1(46Q) control, fibrils were detected after 5 h, and the signal increased after 8 h in htt control. With 1x ruthenium red, no fibrils were detected at 5 h, but fibrils were detected at 8 h, but the staining was considerably less pronounced than control. With 4x ruthenium red, fibrils were not detected at any time point(Figure 2c). These results are consistent with the ThT assays.

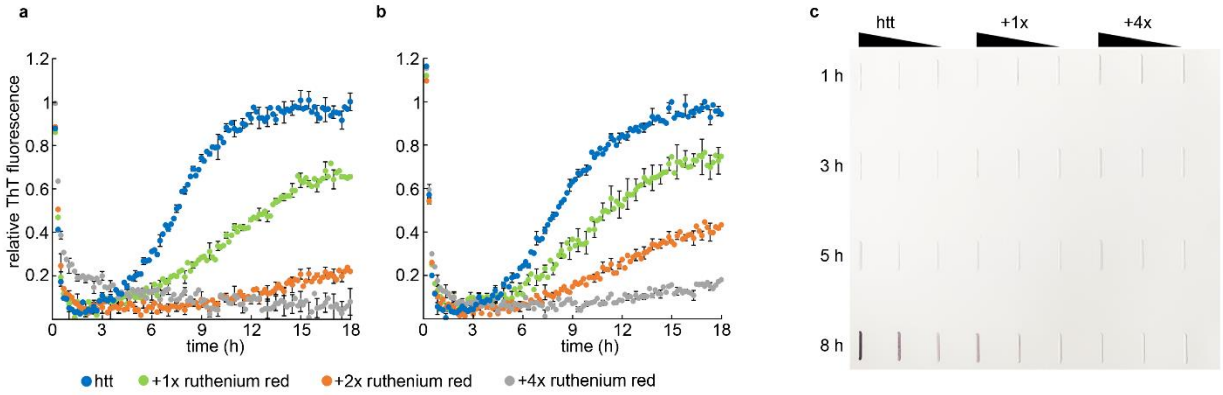

Figure 3.2 Impact of ruthenium red on htt aggregation, **a**, relative Tht fluorescence of htt exon1(46Q) (10 µM) in the presence of varying doses of ruthenium red, **b,** in the presence of TBLE vesicles (htt : TBLE at 1:20). **c,** filter trap assay of htt exon1 (46Q) in the presence of varying doses of ruthenium red. For each condition left to right are three serial dilutions (1.2 µg, 0.6 µg and 0.3 µg of htt). Membrane was probed with anti htt antibody MW8. All Error bars represent SEM.

While ThT and filter trap assays confirm ruthenium red's ability to inhibit htt-exon1(46Q) fibril formation, they do not provide information about aggregate morphology

or changes to oligomer formation. To determine the impact of ruthenium red on htt-exon1(46Q) aggregate morphology, AFM analysis was performed. Htt-exon1(46Q) (10 μM) was incubated with 1x or 4x ruthenium red. Aliquots of these incubations were deposited on mica and imaged with AFM. Incubations of htt-exon1(46Q) without ruthenium red were used as a control. Oligomers appeared at 1 h and 3 h for all conditions. Fibril bundles appeared in the htt-exon1(46Q) control at 5 h and increased in size at 8 h (Figure 3a). While discrete fibrils were present in the control at these time points, most fibrils were incorporated into large bundles. The height of single fibril strands protruding from these bundles were typically in the range of 7.5-9 nm. Due to the stacking of fibrils in bundles, the height of these were often in the 20-30 nm range. In the presence of either 1x or 4x ruthenium red, htt-exon1(46Q) fibrls were observed after 8 h of incubation. However, these were primarily individual fibrils (height across of ~7.5-9 nm) with the occasional small bundle (Figure 3b). To quantify fibril density for each condition in the AFM images, fibril volume per unit area of mica was determined using automated scripts in Matlab, Fibrils were defined as any feature with a height above 1 nm and occupying of an area above 1,000 nm^2. At 8 h the volume covered by fibrils in the presence of either 1x ruthenium red or 4x ruthenium red was significantly reduce compared to htt-exon1(46Q) control. The larger error bars associated with the htt control is due to the presence of large fibril bundles (Figure 3c).

Having established that the fibrilization was suppressed by Ruthenium red, AFM images from the early time points (1 h, 3 h and 5 h) were analyzed to determine if oligomer morphology was altered. Oligomers were defined as any feature greater than 0.8 nm in height and with an aspect ratio less than 2.5 (globular structure) occupying a surface area

< 1000 nm^2. In the absence of ruthenium red, htt-exon1(46Q) oligomers had a mode height of ~2-2.5 nm across the three time points. In contrast, ruthenium red (both 1x and 4x) promoted larger oligomers that were more diverse in size compared to control. For oligomers formed in the presence of 1x ruthenium red, their mode heights were ~2.5-3.5 nm for the 1 and 3 h time point and ~3-4.0 nm for the 8 h time point. With 4x treatment of ruthenium red, oligomers displayed mode heights of ~2.5-4.5 nm for the 1 and 3 h time points, and this swelled to ~3-5 nm after 8 h of incubation (Figure 3d). This swelling in oligomer size may be due to incorporation of ruthenium red into oligomers. This incorporation may increase the distance between polyQ domains in oligomers, reducing the efficiency of fibril formation in a similar mechanism as has been described for Nt17 based peptide inhibitors[55].

3.3.4 Ruthenium red alleviate phenotype in a C. elegans model of HD.

Having established that ruthenium red impacts the ability of htt-exon1(46Q) to bind membranes and alters its aggregation, the impact of ruthenium red on htt-induced toxicity was investigated using a *C. elegans* model of HD. Two *C. elegans* strains were used: EAK102 which express a YFP labeled htt513 fragment with 15 repeat glutamine residues (Q15) and the EAK103 that expresses a YFP htt513 with 128 repeat glutamine residues (Q128)[47]. Htt513 is an N-terminal fragment of the first 513 htt residues (based off a nonpathogenic length polyQ stretch) and is longer that htt-exon1. Importantly, the htt513 fragment contains Nt17, and the YFP tag is placed on the C-terminal side, reducing potential interference with Nt17 function. EAK103 exhibits both a viability and thrashing deficit relative to EAK102[47]. In addition, inclusions readily form in EAK103. After establishing a treated with two doses of ruthenium red (20 µM and 40 µM).

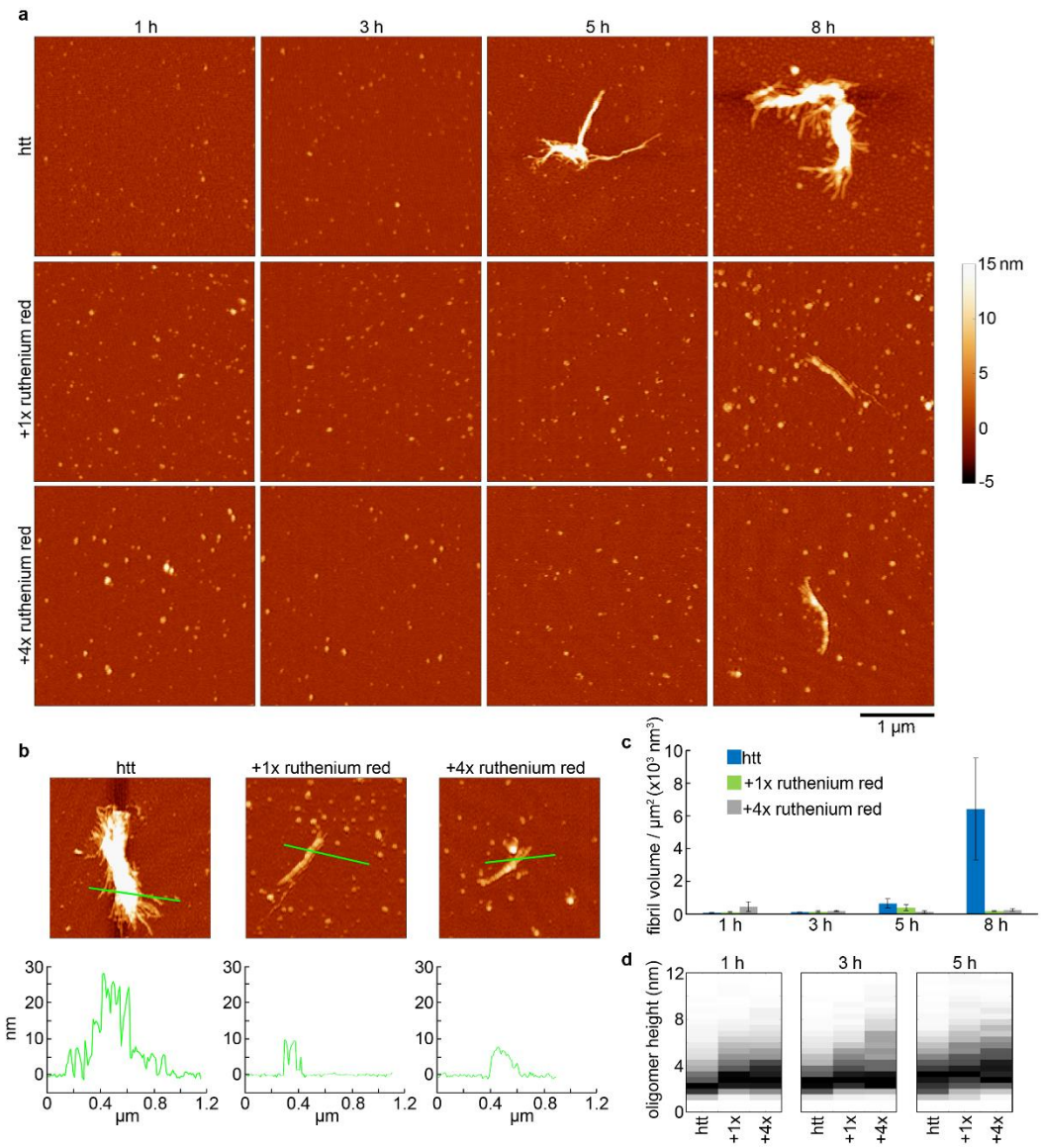

Figure 3.3 Impact of ruthenium red on htt aggregation morphology. a, Representative AFM images of htt exon1 (46Q) (10 µM) incubated alone and in the presence of varying doses of ruthenium red at 37 ^{0}C. **b,** Comparison of the height of htt exon1 (46Q) (10 µM) fibrils and htt exon1 (46Q) (10 µM) fibrils formed in the presence of ruthenium red. The lines on the image correspond to the height profiles directly below the image **c,** Volume occupied by the fibrils per µm^2 based on the AFM images. **d,** Height histogram of the oligomers of htt exon1 (46Q) (10 µM) formed in the presence and absence of ruthenium red for 3 time points (1 h, 3 h and 5 h). Each column in the heat map is normalized by dividing the entire distribution by the number of oligomers in the most populated bin. All Error bars represent SEM.

Both doses of ruthenium red significantly improved the thrashing deficit ($p < 0.05$ for 20 µM and $p < 0.01$ for 40 µM) at day 2 and day 7 (Figure 4a). However, neither dose reduced the formation of visible inclusions in the EAK103 worms based on fluorescent images. This may be due to inclusions forming in worms before they reached the L4 stage. Nevertheless, ruthenium red treatments improved phenotype in EAK103.

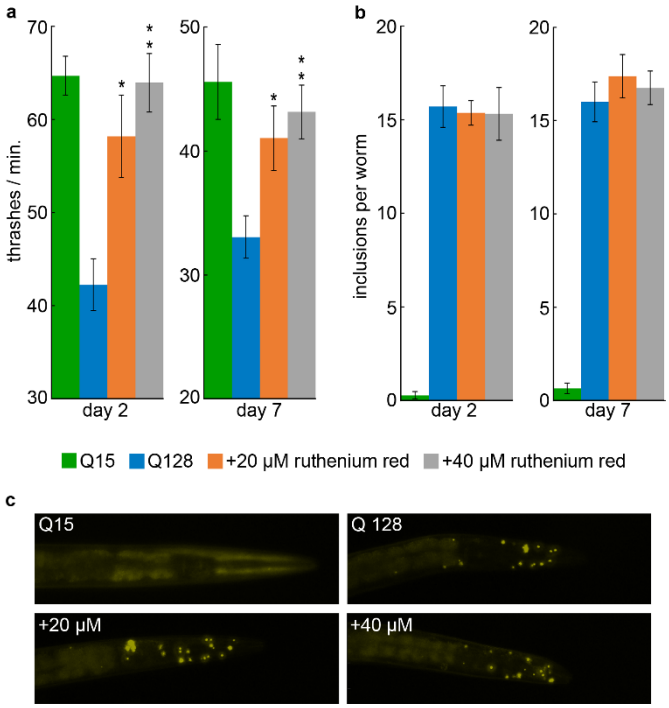

Figure 3.4 Impact of ruthenium red on a C. elegans model of HD, a, Thrashing rate of Q15 worms, Q128 worms and Q128 worms treated with ruthenium red in M9 buffer. Q15 worms were used as a control. **b,** Number of inclusions per worm based on fluorescent microscopic images. **c,** Representative fluorescence images of Q15 worms, Q128 worms and Q128 worms treated with ruthenium red. * indicates $P<0.05$ and ** indicates $P<0.01$. All error bars represent SEM.

3.4 Discussion

For several decades, modulating amyloid formation represents a common strategy to develop therapeutics for amyloid based diseases[8]. While a vast number of aggregation altering agents have been discovered, this approach has yielded few effective drugs for patients[56–58]. For some of these aggregation modifying agents, the presence of lipids causes them to lose their efficacy (in terms of reducing fibril formation) in the presence of lipid membranes. The effective is often protein specific. For instance, EGCG inhibits amyloid formation of Aβ, htt, and human islet amyloid peptide (hIAPP)[52,59–61]. EGCG remains effective at reducing Aβ aggregation in the presence of lipids[62]; however, lipid membranes reduce EGCG's ability to block htt and hIAPP aggregation[52,61]. This could be due to various reasons. Some compounds that block aggregation have significant hydrophobic character that causes them to partition into membranes, preventing them from interacting with proteins[52]. On the other hand, many amyloid-forming proteins directly interact with lipid membranes[18,63,64], and this can promote unique aggregation pathways that may bypass the target of some amyloid inhibitors[24]. Further complicating the issue, preventing aggregation may actually promote or stabilize more toxic intermediate species[65].

While Chapter 2 and studies with squalimine with Aβ and α-synuclein suggest that blocking the ability of amyloid proteins to interact with membranes has potential therapeutic benefit, this approach could be coupled with modifiers of aggregation to attack the toxic action of amyloids on two fronts[66,67]. That is, both approaches may be part of a larger cocktail that together impart benefit to patients. That is, dislodging amyloid proteins from membranes may improve the efficacy of some amyloid inhibitors. Here, ruthenium

red was identified as a compound that blocked the ability of htt to bind membranes and altered aggregation, suggesting some compounds may function in both strategies. For HD specifically, another component of this potential treatment cocktail could be methods to reduce mutant htt expression[68,69]. Several methods to reduce htt expression have gone to clinical trial with limited success so far[70,71]. These methods utilizes a synthetic antisense oligonucleotides that are directly injected into the cerebrospinal fluid[68,69]. Once the antisense oligonucleotides are delivered to the nucleus of the recipient cells in the central nervous system, it binds to htt mRNA resulting degradation, thus lowering the amount of htt[70]. However, mutant htt is still expressed to some level with these strategies. Considering that low concentrations of mutant htt can still aggregate and even seed nonpathogenic htt to aggregate, additional therapies (i.e. blocking lipid binding and aggregation inhibitions) may prove to be important supplements to these htt-expression lowering strategies. In addition, implementation of these methods to reduce htt expression require invasive delivery methods such as routine spinal taps. Perhaps, a combinatorial approach would prolong the period required between treatments.

Ruthenium red is cationic with an overall charge of +6. When charged lipid membranes are present, ruthenium red's ability to suppress htt aggregation and lipid binding may vary despite being effective in the presence of uncharged TBLE. Htt aggregation and interaction with lipid membranes is altered with the type of the lipid, especially when charged head groups are involved[24,72]. For example, anionic lipids such as POPG and POPS enhanced the rate of htt aggregation[72]. Further it is revealed that htt membrane interaction is enhanced by the negative charge of the membrane, i.e. increasing the anionic lipid content in membrane causes a higher interaction[73]. Taken

these facts into consideration and being that ruthenium red is cationic, such a scenario is possible. Therefore, it will be necessary to further explore the efficacy of ruthenium red to block htt membrane-binding (and even aggregation) in the presence of different charged lipid systems. Furthermore, ruthenium red binds to polysaccharides on outer cellular membranes, and multiple Ca^{2+} binding proteins and tubulin[32,34,74]. Due to this non-specificity of ruthenium red, it will likely be challenging to develop it as a drug for HD. However, it can be used to better understand mechanisms associated with htt/membrane interactions and htt aggregation in the presence of membranes. Collectively, this would provide invaluable knowledge in designing agents with the desired specificity.

Despite no effective htt-aggregation blockers being approved to treat HD, some compounds successfully alleviate HD phenotype in multiple animal models. The disaccharide trehalose, small molecule C2-8 which prevents polyQ aggregation invitro, improved striatal atrophy, survival, and motor function in R6/2 mouse model[75,76]. Moreover, polyQ binding peptide QBP1 which suppress polyQ aggregation alleviates neurodegeneration in HD fly model[77]. Neurotoxicity caused by htt is reduced by MW7 antibody that binds to the polyP domain of htt[78]. Thus, there is considerable evidence that blocking aggregation may have therapeutic benefit. In this regard, ruthenium red has the capability to both inhibit htt-lipid interaction as well as subdue aggregation. Furthermore, its efficiency is not altered in the presence of lipid membranes. Again, ruthenium red lacks specificity; however, it does demonstrate that it is possible for a molecule to simultaneously block both the interaction of htt with membranes and aggregation. Perhaps, both modalities should be considered when developing therapeutics that modify amyloid formation.

3.5 References

1. Koo, E. H., Lansbury, P. T. & Kelly, J. W. Amyloid diseases: Abnormal protein aggregation in neurodegeneration. *Proc. Natl. Acad. Sci. U.S.A.* **96**, 9989–9990 (1999).
2. Adegbuyiro, A., Sedighi, F., Pilkington, A. W., Groover, S. & Legleiter, J. Proteins Containing Expanded Polyglutamine Tracts and Neurodegenerative Disease. *Biochemistry* **56**, 1199–1217 (2017).
3. Matiiv, A. B. *et al.* Amyloid and Amyloid-Like Aggregates: Diversity and the Term Crisis. *Biochemistry Moscow* **85**, 1011–1034 (2020).
4. Hirota-Nakaoka, N. Dissolution of 2-Microglobulin Amyloid Fibrils by Dimethylsulfoxide. *Journal of Biochemistry* **134**, 159–164 (2003).
5. Meersman, F. & Dobson, C. M. Probing the pressure–temperature stability of amyloid fibrils provides new insights into their molecular properties. *Biochimica et Biophysica Acta (BBA) - Proteins and Proteomics* **1764**, 452–460 (2006).
6. Ward, R. V. *et al.* Fractionation and characterization of oligomeric, protofibrillar and fibrillar forms of β-amyloid peptide. *Biochemical Journal* **348**, 137–144 (2000).
7. Sathasivam, K. *et al.* Identical oligomeric and fibrillar structures captured from the brains of R6/2 and knock-in mouse models of Huntington's disease. *Human Molecular Genetics* **19**, 65–78 (2010).
8. Zaman, M., Khan, A. N., Wahiduzzaman, Zakariya, S. M. & Khan, R. H. Protein misfolding, aggregation and mechanism of amyloid cytotoxicity: An overview and therapeutic strategies to inhibit aggregation. *International Journal of Biological Macromolecules* **134**, 1022–1037 (2019).
9. Chang, C.-C., Edwald, E., Veatch, S., Steel, D. G. & Gafni, A. Interactions of amyloid-β peptides on lipid bilayer studied by single molecule imaging and tracking. *Biochimica et Biophysica Acta (BBA) - Biomembranes* **1860**, 1616–1624 (2018).
10. Fusco, G. *et al.* Structural basis of membrane disruption and cellular toxicity by α-synuclein oligomers. *Science* **358**, 1440–1443 (2017).
11. Macdonald, M. A novel gene containing a trinucleotide repeat that is expanded and unstable on Huntington's disease chromosomes. *Cell* **72**, 971–983 (1993).
12. Penney, J. B., Vonsattel, J.-P., Macdonald, M. E., Gusella, J. F. & Myers, R. H. CAG repeat number governs the development rate of pathology in Huntington's disease. *Ann Neurol.* **41**, 689–692 (1997).
13. Choo, Y. S. Mutant huntingtin directly increases susceptibility of mitochondria to the calcium-induced permeability transition and cytochrome c release. *Human Molecular Genetics* **13**, 1407–1420 (2004).
14. Panov, A. V. *et al.* Early mitochondrial calcium defects in Huntington's disease are a direct effect of polyglutamines. *Nat Neurosci* **5**, 731–736 (2002).
15. Ueda, M. *et al.* Expanded polyglutamine embedded in the endoplasmic reticulum causes membrane distortion and coincides with Bax insertion. *Biochemical and Biophysical Research Communications* **474**, 259–263 (2016).
16. Bäuerlein, F. J. B. *et al.* In Situ Architecture and Cellular Interactions of PolyQ Inclusions. *Cell* **171**, 179-187.e10 (2017).
17. Liu, K.-Y. *et al.* Disruption of the nuclear membrane by perinuclear inclusions of mutant huntingtin causes cell-cycle re-entry and striatal cell death in mouse and cell models of Huntington's disease. *Human Molecular Genetics* **24**, 1602–1616 (2015).

18. Burke, K. A., Yates, E. A. & Legleiter, J. Biophysical Insights into How Surfaces, Including Lipid Membranes, Modulate Protein Aggregation Related to Neurodegeneration. *Front. Neurol.* **4**, (2013).
19. Burke, K. A., Yates, E. A. & Legleiter, J. Amyloid-Forming Proteins Alter the Local Mechanical Properties of Lipid Membranes. *Biochemistry* **52**, 808–817 (2013).
20. Burke, K. A., Hensal, K. M., Umbaugh, C. S., Chaibva, M. & Legleiter, J. Huntingtin disrupts lipid bilayers in a polyQ-length dependent manner. *Biochimica et Biophysica Acta (BBA) - Biomembranes* **1828**, 1953–1961 (2013).
21. Gao, X. *et al.* Cholesterol Modifies Huntingtin Binding to, Disruption of, and Aggregation on Lipid Membranes. *Biochemistry* **55**, 92–102 (2016).
22. Chaibva, M. *et al.* Sphingomyelin and GM1 Influence Huntingtin Binding to, Disruption of, and Aggregation on Lipid Membranes. *ACS Omega* **3**, 273–285 (2018).
23. Caron, N. S., Desmond, C. R., Xia, J. & Truant, R. Polyglutamine domain flexibility mediates the proximity between flanking sequences in huntingtin. *Proc. Natl. Acad. Sci. U.S.A.* **110**, 14610–14615 (2013).
24. Pandey, N. K. *et al.* The 17-residue-long N terminus in huntingtin controls stepwise aggregation in solution and on membranes via different mechanisms. *Journal of Biological Chemistry* **293**, 2597–2605 (2018).
25. Williamson, T. E., Vitalis, A., Crick, S. L. & Pappu, R. V. Modulation of Polyglutamine Conformations and Dimer Formation by the N-Terminus of Huntingtin. *Journal of Molecular Biology* **396**, 1295–1309 (2010).
26. Darnell, G., Orgel, J. P. R. O., Pahl, R. & Meredith, S. C. Flanking Polyproline Sequences Inhibit β-Sheet Structure in Polyglutamine Segments by Inducing PPII-like Helix Structure. *Journal of Molecular Biology* **374**, 688–704 (2007).
27. Burke, K. A., Kauffman, K. J., Umbaugh, C. S., Frey, S. L. & Legleiter, J. The Interaction of Polyglutamine Peptides with Lipid Membranes Is Regulated by Flanking Sequences Associated with Huntingtin. *Journal of Biological Chemistry* **288**, 14993–15005 (2013).
28. Michalek, M., Salnikov, E. S., Werten, S. & Bechinger, B. Membrane Interactions of the Amphipathic Amino Terminus of Huntingtin. *Biochemistry* **52**, 847–858 (2013).
29. Michalek, M., Salnikov, E. S. & Bechinger, B. Structure and Topology of the Huntingtin 1–17 Membrane Anchor by a Combined Solution and Solid-State NMR Approach. *Biophysical Journal* **105**, 699–710 (2013).
30. Côté, S., Binette, V., Salnikov, E. S., Bechinger, B. & Mousseau, N. Probing the Huntingtin 1-17 Membrane Anchor on a Phospholipid Bilayer by Using All-Atom Simulations. *Biophysical Journal* **108**, 1187–1198 (2015).
31. Côté, S., Wei, G. & Mousseau, N. Atomistic mechanisms of huntingtin N-terminal fragment insertion on a phospholipid bilayer revealed by molecular dynamics simulations: htt $^{NT}Q_N$ Insertion on a Phospholipid Bilayer. *Proteins* **82**, 1409–1427 (2014).
32. Deinum, J., Wallin, M. & Jensen, P. W. The binding of Ruthenium red to tubulin. *Biochimica et Biophysica Acta (BBA) - General Subjects* **838**, 197–205 (1985).
33. Charuk, J. H. M., Pirraglia, C. A. & Reithmeier, R. A. F. Interaction of ruthenium red with Ca2+-binding proteins. *Analytical Biochemistry* **188**, 123–131 (1990).

34. Rossi, C. S., Vasington, F. D. & Carafoli, E. The effect of ruthenium red on the uptake and release of Ca2+ by mitochondria. *Biochemical and Biophysical Research Communications* **50**, 846–852 (1973).
35. Brabec, V. & Nováková, O. DNA binding mode of ruthenium complexes and relationship to tumor cell toxicity. *Drug Resistance Updates* **9**, 111–122 (2006).
36. Kostova, I. Ruthenium Complexes as Anticancer Agents. *CMC* **13**, 1085–1107 (2006).
37. Mohamed Subarkhan, M. K. *et al.* Novel tetranuclear ruthenium(II) arene complexes showing potent cytotoxic and antimetastatic activity as well as low toxicity in vivo. *European Journal of Medicinal Chemistry* **179**, 246–256 (2019).
38. Cuccioloni, M. *et al.* Enhancing the Amyloid-β Anti-Aggregation Properties of Curcumin via Arene-Ruthenium(II) Derivatization. *IJMS* **23**, 8710 (2022).
39. Zhu, D. *et al.* Roles of DMSO-type ruthenium complexes in disaggregation of prion neuropeptide PrP106–126. *RSC Adv.* **6**, 16055–16065 (2016).
40. Zhu, D., Gong, G., Wang, W. & Du, W. Disaggregation of human islet amyloid polypeptide fibril formation by ruthenium polypyridyl complexes. *Journal of Inorganic Biochemistry* **170**, 109–116 (2017).
41. Gong, G., Du, W., Xu, J., Huang, X. & Yin, G. Regulation of heteronuclear Pt–Ru complexes on the fibril formation and cytotoxicity of human islet amyloid polypeptide. *Journal of Inorganic Biochemistry* **189**, 7–16 (2018).
42. Yawson, G. K. *et al.* Ruthenium(III) complexes with imidazole ligands that modulate the aggregation of the amyloid-β peptide via hydrophobic interactions. *Journal of Inorganic Biochemistry* **214**, 111303 (2021).
43. Kumar, A. *et al.* Inhibition of Aβ42 Peptide Aggregation by a Binuclear Ruthenium(II)−Platinum(II) Complex: Potential for Multimetal Organometallics as Anti-amyloid Agents. *ACS Chem. Neurosci.* **1**, 691–701 (2010).
44. Son, G., Lee, B. I., Chung, Y. J. & Park, C. B. Light-triggered dissociation of self-assembled β-amyloid aggregates into small, nontoxic fragments by ruthenium (II) complex. *Acta Biomaterialia* **67**, 147–155 (2018).
45. Thompson, L. M. *et al.* IKK phosphorylates Huntingtin and targets it for degradation by the proteasome and lysosome. *Journal of Cell Biology* **187**, 1083–1099 (2009).
46. Zheng, F., Wu, Z. & Chen, Y. A quantitative method for the measurement of membrane affinity by polydiacetylene-based colorimetric assay. *Analytical Biochemistry* **420**, 171–176 (2012).
47. Lee, A. L., Ung, H. M., Sands, L. P. & Kikis, E. A. A new Caenorhabditis elegans model of human huntingtin 513 aggregation and toxicity in body wall muscles. *PloS one* **12**, e0173644 (2017).
48. Corsi, A. K. A Transparent window into biology: A primer on Caenorhabditis elegans. *WormBook* 1–31 (2015) doi:10.1895/wormbook.1.177.1.
49. Schindelin, J. *et al.* Fiji: an open-source platform for biological-image analysis. *Nat Methods* **9**, 676–682 (2012).
50. Nussbaum-Krammer, C. I., Neto, M. F., Brielmann, R. M., Pedersen, J. S. & Morimoto, R. I. Investigating the Spreading and Toxicity of Prion-like Proteins Using the Metazoan Model Organism C. elegans. *JoVE* 52321 (2015) doi:10.3791/52321.
51. Voelker, D. & Smejtek, P. Adsorption of ruthenium red to phospholipid membranes. *Biophysical Journal* **70**, 818–830 (1996).

52. Beasley, M. *et al.* Lipid Membranes Influence the Ability of Small Molecules To Inhibit Huntingtin Fibrillization. *Biochemistry* **58**, 4361–4373 (2019).
53. Ko, J., Ou, S. & Patterson, P. H. New anti-huntingtin monoclonal antibodies: implications for huntingtin conformation and its binding proteins. *Brain Research Bulletin* **56**, 319–329 (2001).
54. Lin, H.-K. *et al.* Fibril polymorphism affects immobilized non-amyloid flanking domains of huntingtin exon1 rather than its polyglutamine core. *Nat Commun* **8**, 15462 (2017).
55. Mishra, R. *et al.* Inhibiting the Nucleation of Amyloid Structure in a Huntingtin Fragment by Targeting α-Helix-Rich Oligomeric Intermediates. *Journal of Molecular Biology* **415**, 900–917 (2012).
56. Re, F. *et al.* Beta Amyloid Aggregation Inhibitors: Small Molecules as Candidate Drugs for Therapy of Alzheimers Disease. *CMC* **17**, 2990–3006 (2010).
57. Jokar, S. *et al.* Recent advances in the design and applications of amyloid-β peptide aggregation inhibitors for Alzheimer's disease therapy. *Biophys Rev* **11**, 901–925 (2019).
58. Doig, A. J. & Derreumaux, P. Inhibition of protein aggregation and amyloid formation by small molecules. *Current Opinion in Structural Biology* **30**, 50–56 (2015).
59. Bieschke, J. *et al.* EGCG remodels mature α-synuclein and amyloid-β fibrils and reduces cellular toxicity. *Proc. Natl. Acad. Sci. U.S.A.* **107**, 7710–7715 (2010).
60. Palhano, F. L., Lee, J., Grimster, N. P. & Kelly, J. W. Toward the Molecular Mechanism(s) by Which EGCG Treatment Remodels Mature Amyloid Fibrils. *J. Am. Chem. Soc.* **135**, 7503–7510 (2013).
61. Engel, M. F. M. *et al.* The Polyphenol EGCG Inhibits Amyloid Formation Less Efficiently at Phospholipid Interfaces than in Bulk Solution. *J. Am. Chem. Soc.* **134**, 14781–14788 (2012).
62. Malishev, R. *et al.* Toxicity Inhibitors Protect Lipid Membranes from Disruption by Aβ42. *ACS Chem. Neurosci.* **6**, 1860–1869 (2015).
63. Janson, J., Ashley, R. H., Harrison, D., McIntyre, S. & Butler, P. C. The mechanism of islet amyloid polypeptide toxicity is membrane disruption by intermediate-sized toxic amyloid particles. *Diabetes* **48**, 491–498 (1999).
64. Khemtémourian, L., Antoinette Killian, J., Höppener, J. W. M. & Engel, M. F. M. Recent Insights in Islet Amyloid Polypeptide-Induced Membrane Disruption and Its Role in β -Cell Death in Type 2 Diabetes Mellitus. *Experimental Diabetes Research* **2008**, 1–9 (2008).
65. Cheng, I. H. *et al.* Accelerating Amyloid-β Fibrillization Reduces Oligomer Levels and Functional Deficits in Alzheimer Disease Mouse Models. *Journal of Biological Chemistry* **282**, 23818–23828 (2007).
66. Limbocker, R. *et al.* Squalamine and trodusquemine: two natural products for neurodegenerative diseases, from physical chemistry to the clinic. *Nat. Prod. Rep.* **39**, 742–753 (2022).
67. Perni, M. *et al.* A natural product inhibits the initiation of α-synuclein aggregation and suppresses its toxicity. *Proc. Natl. Acad. Sci. U.S.A.* **114**, (2017).
68. Estevez-Fraga, C., Rodrigues, F. B., Tabrizi, S. J. & Wild, E. J. Huntington's Disease Clinical Trials Corner: April 2022. *JHD* **11**, 105–118 (2022).
69. Ferguson, M. W. *et al.* Current and Possible Future Therapeutic Options for Huntington's Disease. *J Cent Nerv Syst Dis* **14**, 117957352210925 (2022).

70. Evers, M. M. & Konstantinova, P. AAV5-miHTT gene therapy for Huntington disease: lowering both huntingtins. *Expert Opinion on Biological Therapy* **20**, 1121–1124 (2020).
71. Spronck, E. *et al.* Intrastriatal Administration of AAV5-miHTT in Non-Human Primates and Rats Is Well Tolerated and Results in miHTT Transgene Expression in Key Areas of Huntington Disease Pathology. *Brain Sciences* **11**, 129 (2021).
72. Beasley, M., Groover, S., Valentine, S. J. & Legleiter, J. Lipid headgroups alter huntingtin aggregation on membranes. *Biochimica et Biophysica Acta (BBA) - Biomembranes* **1863**, 183497 (2021).
73. Tao, M., Pandey, N. K., Barnes, R., Han, S. & Langen, R. Structure of Membrane-Bound Huntingtin Exon 1 Reveals Membrane Interaction and Aggregation Mechanisms. *Structure* **27**, 1570-1580.e4 (2019).
74. Fassel, T. A. & Edmiston, C. E. Ruthenium Red and the Bacterial Glycocaly. *Biotechnic & Histochemistry* **74**, 194–212 (1999).
75. Tanaka, M. *et al.* Trehalose alleviates polyglutamine-mediated pathology in a mouse model of Huntington disease. *Nat Med* **10**, 148–154 (2004).
76. Chopra, V. *et al.* A small-molecule therapeutic lead for Huntington's disease: Preclinical pharmacology and efficacy of C2-8 in the R6/2 transgenic mouse. *Proc. Natl. Acad. Sci. U.S.A.* **104**, 16685–16689 (2007).
77. Nagai, Y. Prevention of polyglutamine oligomerization and neurodegeneration by the peptide inhibitor QBP1 in Drosophila. *Human Molecular Genetics* **12**, 1253–1259 (2003).
78. Southwell, A. L. *et al.* Intrabodies Binding the Proline-Rich Domains of Mutant Huntingtin Increase Its Turnover and Reduce Neurotoxicity. *J. Neurosci.* **28**, 9013–9020 (2008).

Chapter 4 Future directions

4.1 Inhibition of htt lipid interaction serves as a therapeutic strategy.

Aggregation of proteins into amyloid deposits is a major hallmark of many neurodegenerative diseases. The aggregation process is complex, leading to a heterogeneous mixture of aggregates. Many of these aggregates appear toxic. Therefore, over the past decades numerous candidate therapeutics that suppress or alter amyloid aggregation have been developed. This approach has yet to yield an approved therapeutic. However, many amyloid proteins directly interact with lipids, resulting in membrane damage and dysfunction. Here, we present a novel therapeutic strategy: inhibiting the lipid interactions of amyloid forming protein. In chapter 2, a screen was performed using over 1200 compounds and identified 15 candidate compounds that inhibit htt binding to membranes. To validate these candidate compounds, secondary assays were conducted, verifying that six compounds. Of these compounds, Ro-90-7501 (Ro) and Benzamil hydrochloride (Ben) were explored in detail. Both Ro and Ben did not alter htt fibrilization. Mechanism of action of each compound was determined using molecular dynamic simulations and experimentally validated. Both Ro and Ben rescued phenotype in a *C.elegans* model of HD. In chapter 3, ruthenium red, which was another hit compound identified from the screens, was investigated. Unlike Ro and Ben, ruthenium red suppressed htt fibril formation while inhibiting lipid interaction. It also rescued phenotype in the *C. elegans* model of HD. Collectively, these studies provide proof of concept that inhibiting amyloid/membrane interactions may be a viable therapeutic strategy.

4.2 Exploring indirect impact of drugs in animal models

While the compounds studied here improved phenotype in *C. elegans,* this is only the beginning of developing therapeutics based on this principle. In addition to their ability to inhibit htt/lipid interactions, these compounds, as known pharmacologically active compounds, have other cellular impacts. Ro inhibits the activity of protein phosphatase 5 in a TPR dependent manner suggesting that Ro interacts with TPR domains[1]. Moreover Ro inhibits the activity of human cytomrgalovirus and carbapenem-resistant Enterobacteriaceae via DNA interaction[2,3]. Ben is an amiloride derivative, is an acid sensing ion channel blocker[4,5]. Ruthenium red binds to multiple proteins, especially Ca^{2+} binding proteins[6–8]. It is possible that these compounds have indirect impact in *C.elegans* that resulted the phenotypic change. To obtain a deeper understanding about the changes in protein expression, a proteomic study can be performed. EAK 103 (*C.elegans* expressing 128 glutamines referred to as Q128 in chapter 2 and 3) can be treated with multiple doses Ro, Ben and ruthenium red and a comparison of the total proteome can be performed with respect to untreated worms. EAK 102 (*C.elegans* expressing 15 glutamines referred to as Q15 in chapter 2 and 3) can be used as a control for further comparison.

There are several other mammalian models developed to recapitulate HD phenotype. Of interest is the transgenic mouse model R6/2 that overexpresses htt-exon1 with an expanded polyQ domain (141Q-157Q)[9]. In these mice behavioral abnormalities appear as early as 5–6 weeks of age and early death observed at 10–13 weeks[9]. The mice demonstrate severe HD phenotype such as weight loss, clasping, tremor and

convulsions[9–11]. Another interesting HD model is a knockin pig model that expresses full length htt[12]. Body weight loss, behavioral abnormalities, and early death are observed in these animals in comparison to wild type[12]. To further validate the efficiency of Ro, Ben, and ruthenium red, these animal models can used to investigate their efficacy in improving HD phenotype in mammalian systems.

4.3 Inhibition of lipid binding as a part of solution in a combinatory approach

While the compounds investigated here improved phenotype in *C. elegans* without reducing the formation of htt inclusions, this strategy may not be sufficient alone to combat HD. Rather, a combinatorial approach that takes advantage of several strategies may be warranted. Other strategies being investigated to treat HD include aggregation inhibitors and lowering expression of mutant htt. These treatments strategies are not mutually exclusive and may work synergistically to combat HD. Similar combinatorial approaches may prove appropriate for other amyloid-based neurodegenerative diseases.

Since mutant htt with an expanded polyQ domain is the main culprit in HD, numerous approaches are being implemented to lower mutant htt expression levels to alter disease progression[13]. Therapeutics at the clinical trial stage use synthetic antisense oligonucleotides that are directly injected into the cerebrospinal fluid[14,15]. Once the antisense oligonucleotides are delivered to the nucleus of the recipient cells in the central nervous system, it binds to htt mRNA, resulting in degradation and lowering the amount of htt[16]. Another approach is the utilizing of gene therapy, which is the use of engineered vectors as delivery vehicles for therapeutics. Most recent gene therapy for HD is using an adeno associated virus vector stereotype 5 (AAV5) that is delivered to the striatum of the brain[16]. In these AAV5 vectors, a transgene that expresses an engineered small RNA

molecule is incorporated that binds to htt mRNA preventing its translation into toxic huntingtin protein[16,17]. While success in lowing mutant htt levels in patients has been modest in clinical trials, these strategies require invasive, regular spinal taps. Reducing the innate toxicity of expressed mutant htt via inhibiting its ability to damage membranes may boost the effectiveness of modest reduction in htt expression and/or may extend the time required between spinal taps.

Since aggregation of htt numerous types of fibrillar aggregates and deposits in cells is the major hallmark of HD, immense effort has been taken over the past decades to develop therapeutics that suppress aggregation. Even though inhibiting aggregation has not led to viable therapeutics, there are multiple studies that demonstrate some of these compounds successfully alleviate HD phenotype in animal models. The disaccharide trehalose, small molecule C2-8 which prevents polyQ aggregation *in vitro*, improved striatal atrophy, survival, and motor function in R6/2 mouse model[18,19]. Moreover, polyQ binding peptide QBP1 which suppress polyQ aggregation alleviates neurodegeneration in HD fly model[20]. Some aggregation inhibitors, however, are ineffective in the presence of lipids. Introducing compounds that reduce the ability of htt to bind membranes may ultimately increase the effectiveness of aggregation blockers. Compounds like ruthenium red may also be able to perform both of these functions, attacking toxic mechanisms on two fronts.

4.4 A roadmap to identify therapeutics for amyloid based diseases.

Inhibiting amyloid protein interactions with lipid membranes can be applied to other amyloid-based diseases as well. Aggregation is altered in the presence of lipid in many amyloid-forming proteins. Moreover, amyloid-forming proteins and their aggregates bind

and physically damages membranes. Steroids squalamine and trodusquemine, alleviate α-synuclein and Aβ toxicity associated with PD and AD respectively by changing membrane properties. Here in our study, we specifically target htt protein for a direct amyloid lipid interaction. This approach can be extended for other amyloid based diseases. We have created a roadmap from the discovery to determining their effectiveness (Figure 5.1).

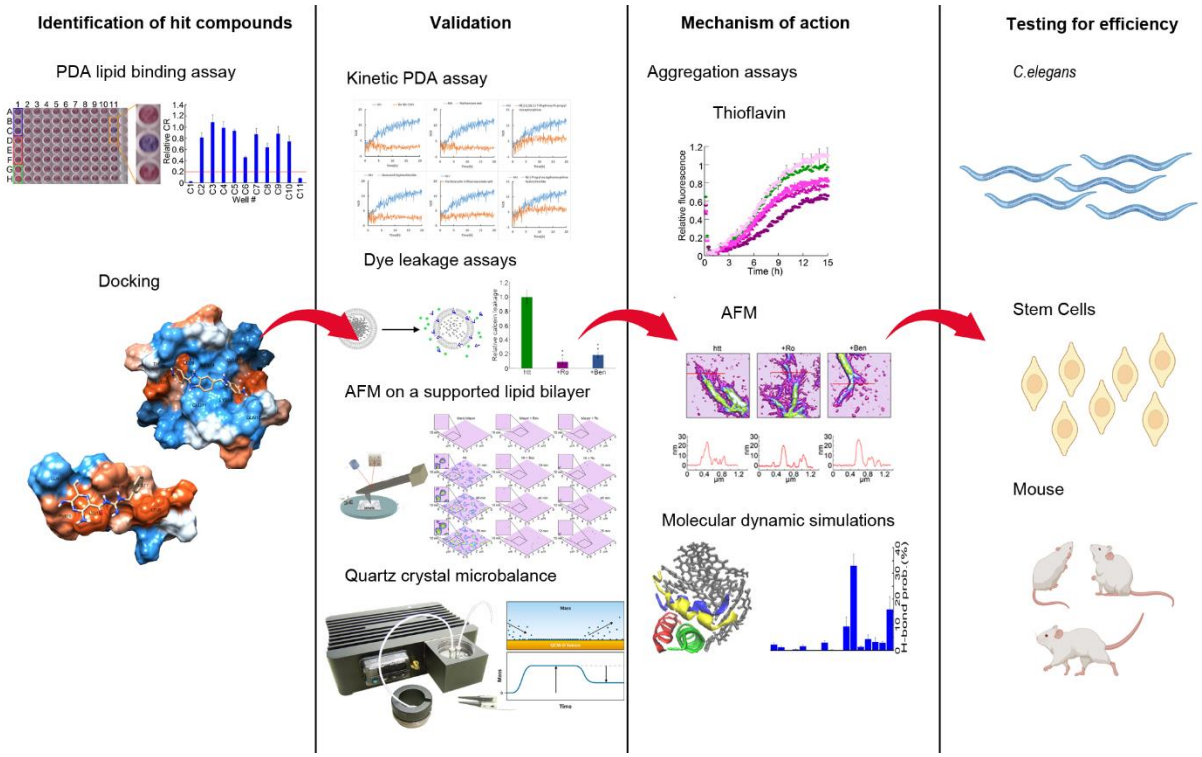

Figure 4.1 Schematic representation of the roadmap for drug identification for amyloid based diseases, a stepwise process starting from hit identification, validation, determining the mechanism and accessing the efficiency.

The first step involves in the identification of candidate compounds via a PDA lipid-binding assay. The advantage of this approach is that it will only identify compounds that directly interact with the protein, as interaction with the lipid vesicle would induce a response in the PDA. This enhances specificity to the disease-associated protein and

prevents potentially harmful changes to lipid membranes associated with a compound. If the lipid-binding domain of the protein is known, molecular docking can be performed to identify hit compounds as an alternative method. Once hit compounds are identified they need to be further validated. Here, kinetic PDA assays, calcein dye leakage assays and *in situ* AFM were used for validation. However, other techniqes may prove useful, e.g. a quartz crystal microbalance. Upon validation, the mechanism of interaction of the compounds with the protein can be determined via additional biophysical characterization. Since amyloids form aggregates with β-sheet rich structures, ThT assay can determine if compounds also impact aggregation. *Ex-situ* AFM can reveal compound induced changes in aggregate morphology and formation. Molecular dynamic simulations can provide detail of potential mechanism of action such as binding sites, binding probability etc. Results from simulations can be used to design further experiments to determine mechanism. The final step is determining if there is potential therapeutic benefit. This can be achieved via cell culture and model organisms to determine if compounds reduce toxicity or improve phenotype. With HD, stem cells from patients represents an interesting system for further investigation. Collectively, the studies presented in this dissertation suggest that blocking the ability of amyloid-forming proteins to interact with membranes is a viable therapeutic avenue.

4.5 References

1. Hong, T.-J., Park, K., Choi, E.-W. & Hahn, J.-S. Ro 90-7501 inhibits PP5 through a novel, TPR-dependent mechanism. *Biochemical and Biophysical Research Communications* **482**, 215–220 (2017).
2. Falci Finardi, N. *et al.* Identification and characterization of bisbenzimide compounds that inhibit human cytomegalovirus replication. *Journal of General Virology* **102**, (2021).

3. Zulauf, K. E. & Kirby, J. E. Discovery of small-molecule inhibitors of multidrug-resistance plasmid maintenance using a high-throughput screening approach. *Proc. Natl. Acad. Sci. U.S.A.* **117**, 29839–29850 (2020).
4. Wang, X., Takeya, K., Aaronson, P. I., Loutzenhiser, K. & Loutzenhiser, R. Effects of amiloride, benzamil, and alterations in extracellular Na^+ on the rat afferent arteriole and its myogenic response. *American Journal of Physiology-Renal Physiology* **295**, F272–F282 (2008).
5. Nishimura, M., Ohtsuka, K., Nanbu, A., Takahashi, H. & Yoshimura, M. Benzamil blockade of brain Na^+ channels averts Na^+ -induced hypertension in rats. *American Journal of Physiology-Regulatory, Integrative and Comparative Physiology* **274**, R635–R644 (1998).
6. Deinum, J., Wallin, M. & Jensen, P. W. The binding of Ruthenium red to tubulin. *Biochimica et Biophysica Acta (BBA) - General Subjects* **838**, 197–205 (1985).
7. Charuk, J. H. M., Pirraglia, C. A. & Reithmeier, R. A. F. Interaction of ruthenium red with Ca2+-binding proteins. *Analytical Biochemistry* **188**, 123–131 (1990).
8. Rossi, C. S., Vasington, F. D. & Carafoli, E. The effect of ruthenium red on the uptake and release of Ca2+ by mitochondria. *Biochemical and Biophysical Research Communications* **50**, 846–852 (1973).
9. Mangiarini, L. *et al.* Exon 1 of the HD gene with an expanded CAG repeat is sufficient to cause a progressive neurological phenotype in transgenic mice. *Cell* **87**, 493–506 (1996).
10. Carter, R. J. *et al.* Characterization of Progressive Motor Deficits in Mice Transgenic for the Human Huntington's Disease Mutation. *J. Neurosci.* **19**, 3248–3257 (1999).
11. Hurlbert, M. S. *et al.* Mice transgenic for an expanded CAG repeat in the Huntington's disease gene develop diabetes. *Diabetes* **48**, 649–651 (1999).
12. Yan, S. *et al.* A Huntingtin Knockin Pig Model Recapitulates Features of Selective Neurodegeneration in Huntington's Disease. *Cell* **173**, 989-1002.e13 (2018).
13. Miniarikova, J. *et al.* Design, Characterization, and Lead Selection of Therapeutic miRNAs Targeting Huntingtin for Development of Gene Therapy for Huntington's Disease. *Molecular Therapy - Nucleic Acids* **5**, e297 (2016).
14. Estevez-Fraga, C., Rodrigues, F. B., Tabrizi, S. J. & Wild, E. J. Huntington's Disease Clinical Trials Corner: April 2022. *JHD* **11**, 105–118 (2022).
15. Ferguson, M. W. *et al.* Current and Possible Future Therapeutic Options for Huntington's Disease. *J Cent Nerv Syst Dis* **14**, 117957352210925 (2022).
16. Evers, M. M. & Konstantinova, P. AAV5-miHTT gene therapy for Huntington disease: lowering both huntingtins. *Expert Opinion on Biological Therapy* **20**, 1121–1124 (2020).
17. Spronck, E. *et al.* Intrastriatal Administration of AAV5-miHTT in Non-Human Primates and Rats Is Well Tolerated and Results in miHTT Transgene Expression in Key Areas of Huntington Disease Pathology. *Brain Sciences* **11**, 129 (2021).
18. Tanaka, M. *et al.* Trehalose alleviates polyglutamine-mediated pathology in a mouse model of Huntington disease. *Nat Med* **10**, 148–154 (2004).
19. Chopra, V. *et al.* A small-molecule therapeutic lead for Huntington's disease: Preclinical pharmacology and efficacy of C2-8 in the R6/2 transgenic mouse. *Proc. Natl. Acad. Sci. U.S.A.* **104**, 16685–16689 (2007).

20. Nagai, Y. Prevention of polyglutamine oligomerization and neurodegeneration by the peptide inhibitor QBP1 in Drosophila. *Human Molecular Genetics* **12**, 1253–1259 (2003).